Variability in sediment particle size, mineralogy, and Fe mode of occurrence across dust-source inland drainage basins: the case of the lower Drâa Valley, Morocco

Adolfo González-Romero[1,2,3], Cristina González-Florez[1,3], Agnesh Panta[4], Jesús Yus-Díez[2,a], Cristina Reche[2], Patricia Córdoba[2], Natalia Moreno[2], Andres Alastuey[2], Konrad Kandler[4], Martina Klose[5], Clarissa Baldo[6], Roger N. Clark[7], Zong Bo Shi[8], Xavier Querol[2], and Carlos Pérez García-Pando[1,9]

[1]Barcelona Supercomputing Center (BSC), Barcelona, Spain
[2]Spanish Research Council, Institute of Environmental Assessment and water Research (IDAEA-CSIC), Barcelona, Spain
[3]Polytechnical University of Catalonia (UPC), Barcelona, Spain
[4]Institute of Applied Geosciences, Technical University Darmstadt, Darmstadt, Germany
[5]Department Troposphere Research, Karlsruhe Institute of Technology (KIT), Institute of Meteorology and Climate Research (IMK-TRO), Karlsruhe, Germany
[6]Université Paris Cité and Univ Paris Est Creteil, CNRS, LISA, 75013 Paris, France
[7]PSI Planetary Science Institute, Tucson, AZ, USA
[8]School of Geography Earth and Environmental Sciences, University of Birmingham, Birmingham, United Kingdom
[9]Catalan Institution for Research and Advanced Studies (ICREA), Barcelona, Spain
[a]now at: Center for Atmospheric Research, University of Nova Gorica, Ajdovščina, Slovenia

Correspondence: Adolfo González-Romero (agonzal3@bsc.es) and Xavier Querol (xavier.querol@idaea.csic.es)

Received: 26 May 2023 – Discussion started: 7 June 2023
Revised: 28 August 2023 – Accepted: 2 October 2023 – Published:

Abstract. The effects of desert dust upon climate and ecosystems depend strongly on its particle size and size-resolved mineralogical composition. However, there is very limited quantitative knowledge on the particle size and composition of the parent sediments along with their variability within dust-source regions, particularly in dust emission hotspots. The lower Drâa Valley, an inland drainage basin and dust hotspot region located in the Moroccan Sahara, was chosen for a comprehensive analysis of sediment particle size and mineralogy. Different sediment type samples ($n = 42$) were collected, including paleo-sediments, paved surfaces, crusts, and dunes, and analysed for particle-size distribution (minimally and fully dispersed samples) and mineralogy. Furthermore, Fe sequential wet extraction was carried out to characterise the modes of occurrence of Fe, including Fe in Fe (oxyhydr)oxides, mainly from goethite and hematite, which are key to dust radiative effects; the poorly crystalline pool of Fe (readily exchangeable ionic Fe and Fe in nano-Fe oxides), relevant to dust impacts upon ocean biogeochemistry; and structural Fe. Results yield a conceptual model where both particle size and mineralogy are segregated by transport and deposition of sediments during runoff of water across the basin and by the precipitation of salts, which causes a sedimentary fractionation. The proportion of coarser particles enriched in quartz is higher in the highlands, while that of finer particles rich in clay, carbonates, and Fe oxides is higher in the lowland dust emission hotspots. There, when water ponds and evaporates, secondary carbonates and salts precipitate, and the clays are enriched in readily exchangeable ionic Fe, due to sorption of dissolved

Proof only

Fe by illite. The results differ from currently available mineralogical atlases and highlight the need for observationally constrained global high-resolution mineralogical data for mineral-speciated dust modelling. The dataset obtained represents an important resource for future evaluation of surface mineralogy retrievals from spaceborne spectroscopy.

1 Introduction

Desert dust is atmospheric particulate matter (PM), mostly mineral in composition, emitted by wind erosion of arid and semi-arid surfaces. The global dust-source regions include northern Africa, the Middle East, central Asia, western Australia, South America, southern Africa, and southern United States–northern Mexico. These regions include most of the so-called dust emission "hotspots", defined as localised, persistent areas of intense dust production within an overall landscape which generally does not emit dust (Gillette, 1999; Baddock et al., 2016). Northern Africa accounts for around 50 % of global dust emissions, followed by central Asia, the Middle East, and eastern Asia (Kok et al., 2021). Dust storms arise when strong winds generate a large number of dust particles that drastically reduce visibility nearby and are transported over distances of hundreds of kilometres (Prospero et al., 2002). During transport, dust perturbs the energy and water cycles by direct radiative forcing and influences cloud formation, precipitation, and the associated indirect radiative forcing (Weaver et al., 2002). Dust transports nutrients across the planet, affecting ocean productivity (Boyd et al., 2007), plant nutrient gain or loss (Sullivan et al., 2007; Doronzo et al., 2016; Alshemmari et al., 2013; Al-Dousari et al., 2020), and glacier mass budgets (Goudie and Middleton, 2006). Dust can also directly affect human health by inhalation or by favouring the propagation of diseases (Goudie and Middleton, 2006; De Longueville et al., 2010; Karanasiou et al., 2012; Pérez García-Pando et al., 2014; Al-Dousari et al., 2018). It can reduce renewable solar energy output due to the attenuation of solar radiation and soiling of solar panels (Al-Dousari et al., 2019; Monteiro et al., 2022); create poor visibility on roads, increasing the risk of traffic accidents (Middleton, 2017); and cause disturbances in airport operations and air traffic (Monteiro et al., 2022).

Dust is emitted mostly from arid inland drainage basins (Prospero et al., 2002; Goudie and Middleton, 2006; Bullard et al., 2011; Querol et al., 2019). These basins encompass different sedimentary environments, many of which are potentially dust emission hotspots, including unconsolidated aeolian deposits, endorheic depressions, and fluvial- and alluvial-dominated systems (Bullard et al., 2011). Consolidated or compacted fine sediments in the form of crusts and paved sediments, for instance on ephemeral lake beds, can also be important dust emitting surfaces when loose sand size sediments provided by adjacent sand dunes are available (Stout and Lee, 2003). These sand particles are efficiently mobilised by wind and blast the consolidated surface, breaking the sediment aggregates and releasing dust (Shao et al., 2011).

Models developed to simulate the atmospheric dust cycle and its impact on climate represent dust emission, transport, interactions with radiation and clouds, and removal by wet and dry deposition (Ginoux et al., 2001; Zender et al., 2004; Pérez et al., 2011; Klose et al., 2021). The characterisation of dust sources and hotspots is one of the crucial aspects for representing dust mobilisation in models. Initially, models used vegetation cover as a criterion to identify potential dust sources (e.g. Tegen and Fung, 1994). Satellite retrievals subsequently showed that the most prolific sources occupy a smaller fraction of arid regions (Prospero et al., 2002; Ginoux et al., 2012). These so-called hotspots or "preferential sources" are found within enclosed basins, where easily eroded soil particles accumulate after fluvial erosion and transport from the surrounding highlands. The implementation of preferential source functions in global models based on topography (Ginoux et al., 2001), hydrology (Tegen et al. 2002; Zender et al., 2003), geomorphology (Bullard et al., 2011), or satellite proxies (Prospero et al., 2002; Ginoux et al., 2012) has significantly improved the skill of models by approximately locating large-scale natural sources. However, models are not able yet to capture the small-scale spatial and temporal variability in emissions apparent from observations. Models assume relatively homogeneous soil properties due to the lack of data, while there can be significant heterogeneity. Some studies have provided small-scale understanding on the role of geomorphology and sedimentology in dust emissions (Bullard et al., 2011; Baddock et al., 2016). For instance, Bullard et al. (2011) developed a conceptual model of how different geomorphologic surfaces affect the intensity and temporal variability in dust emissions.

While it is key to understand dust hotspot locations and emission intensity, climate impacts by dust also depend upon its mineralogy (Alshemmari et al., 2013). Dust is a mixture of different minerals including quartz; clay minerals (mica / illite, kaolinite, palygorskite, chlorite / clinochlore, and smectite / montmorillonite); feldspars (albite / anorthite and orthoclase); carbonate minerals (mainly calcite and dolomite); salts (mainly halite and gypsum); Fe oxides and hydroxides (mostly goethite and hematite); and other oxides or hydroxides of Ti, Mn, and Al (Caquineau et al., 1998; Claquin et al., 1999; Al-Ghadban et al., 1999; Cattle et al., 2002; Formenti et al., 2008; Nickovic et al., 2012; Alshemmari et al., 2013, Scheuvens et al., 2013; Journet et al., 2014;

Proof Only

Scanza et al., 2015; Subramaniam et al., 2015; Doronzo et al., 2016; Al-Dousari et al., 2018, 2019, 2020; Ito and Wagai, 2017; Querol et al., 2019). The relative abundances, size, shape, and mixing state of these minerals influence the effect of dust upon climate. For instance, the absorption of solar radiation by dust depends upon the iron oxide content (Sokolik and Toon, 1999; Reynolds et al., 2014; Di Biagio et al., 2019), ice nucleation in mixed-phase clouds is highly sensitive to the amount of K-feldspar and quartz (Boose et al., 2016; Harrison et al., 2019), and the bioavailability of iron in dust depends upon its iron mineralogy and speciation (Shi et al., 2012). Recent studies have shown that cloud pH is controlled in great part by calcite from dust (Grider et al., 2023). Furthermore, Ca controls heterogeneous reactions of acids on the surface of dust, which ultimately affect O_3 production (Bauer et al., 2004; Paulot et al., 2016). According to the geological, geomorphological, and climate (weathering) patterns of the desert regions, the type and proportions of minerals might greatly vary (Caquineau et al., 1998; Claquin et al., 1999; among others). For instance, Sahelian dust is composed mainly of quartz, kaolinite, and hematite; Middle Eastern dust is dominated by quartz and carbonates (Al-Dousari, 2018, 2019, 2020); and in dust from north-eastern China and the Sahara, mica / illite, kaolinite, quartz, and carbonates prevail (Shen et al., 2009; Claquin et al., 1999).

Despite the potential importance of dust mineralogical variations, climate models typically assume dust composition as globally uniform, which is partly due to the limited knowledge of the composition of the parent sources at global scale. The few models that explicitly represent dust mineralogical composition (e.g. Scanza et al., 2015; Perlwitz et al., 2015; Li et al., 2021; Gonçalves Ageitos et al., 2023) use global atlases of soil type and the relation of this variable to soil mineralogy. This relation is inferred using massive extrapolation from a limited number of mineralogical analyses, particularly in dust hotspots; ancillary information on soil texture and colour; and a number of additional assumptions (Claquin et al., 1999; Journet et al., 2014). Conventionally, the particle size of dust is characterised by measuring two particle-size ranges, i.e. clay ($< 2\,\mu m$) and silt (2–63 µm), linked to FAO (Food and Agricultural Organization of the United States) soil texture datasets based on measurements following wet sieving, a technique that disperses (breaks up) the mineral aggregates found in the undisturbed parent soil into smaller particles (Chatenet et al., 1996). Furthermore, the samples that underpin these atlases consider the first 10–15 cm of soil sediment, which is much deeper than the thin layer that is relevant to wind erosion and dust emission, and mineralogy is normally analysed after removing organic matter with hydrogen peroxide (H_2O_2), which can partially dissolve carbonate minerals.

The assumed relationship between mineralogy and soil type in these atlases neglects the role of geomorphology and sedimentology affecting the formation of different dust-emitting surface sediments, such as crusts and paved sediments. This study provides a comprehensive analysis of the variability in particle size, mineralogical composition, and Fe mode of occurrence of sediments collected across the lower Drâa Valley, an inland drainage basin and prolific dust source located on the north-western border of the Saharan desert in southern Morocco (Fig. 1). The data collection was carried out during a dust field campaign in September 2019 in the context of the FRontiers in dust minerAloGical coMposition and its Effects upoN climaTe (FRAGMENT) project. Based on the analysis of the results, a conceptual model is proposed that links formation processes of potential dust-emitting sediments to their particle-size distribution (PSD) and mineralogy across the basin.

2 Methodology

2.1 The FRAGMENT field campaign and the study area

The sediment samples analysed in this study were collected during a field campaign that took place in September 2019 in the lower Drâa Valley, west of M'Hamid, between Erg Chigaga and L'Bour (Fig. 1a), a dry inland drainage basin where dust emission is frequent, as evidenced by satellite data (Ginoux et al., 2012) (Fig. 1b). The region lies where the Sahara begins, to the south of the Atlas Mountain, near the Algerian border, in the Drâa River basin. Preliminary results from the Earth Surface Mineral Dust Source Investigation, EMIT (Green et al., 2020), show the presence of a complex regional mineralogy with fine-grained goethite, hematite (with substantial nano-sized hematite), gypsum sulfate salts in the lowlands (depressions), and illite / muscovite, with local outcrops of carbonates in the study area (Fig. 1c). The EMIT mineral maps show that the study area is representative of the larger area.

The campaign was conducted in the framework of the FRAGMENT project, in which distinct desert dust hotspot regions are being characterised to better understand the size-resolved dust emission and composition for different meteorological and soil conditions. The aim of FRAGMENT is to better understand dust emission, its mineralogical composition, and the effects of dust upon climate, by combining field measurements, laboratory analyses, remote and in situ spectroscopy, theory, and modelling. FRAGMENT field campaigns consist of intensive sediment sampling and meteorological and airborne dust measurements in one specific location, along with sediment sampling across the broader basin. The intensive meteorological and airborne dust measurements were performed in the dry lake of L'Bour and are analysed in, for example, González-Flórez et al. (2023), Panta et al. (2023), and Yus-Díez et al. (2023). Here the focus is on the sediment sampling across the basin.

The study area records very low annual precipitation (80 mm) and extremely variable droughts interrupted by extreme flooding (Berger et al., 2021). The Drâa River was anthropogenically dried in this area mostly due to the construc-

Proof only

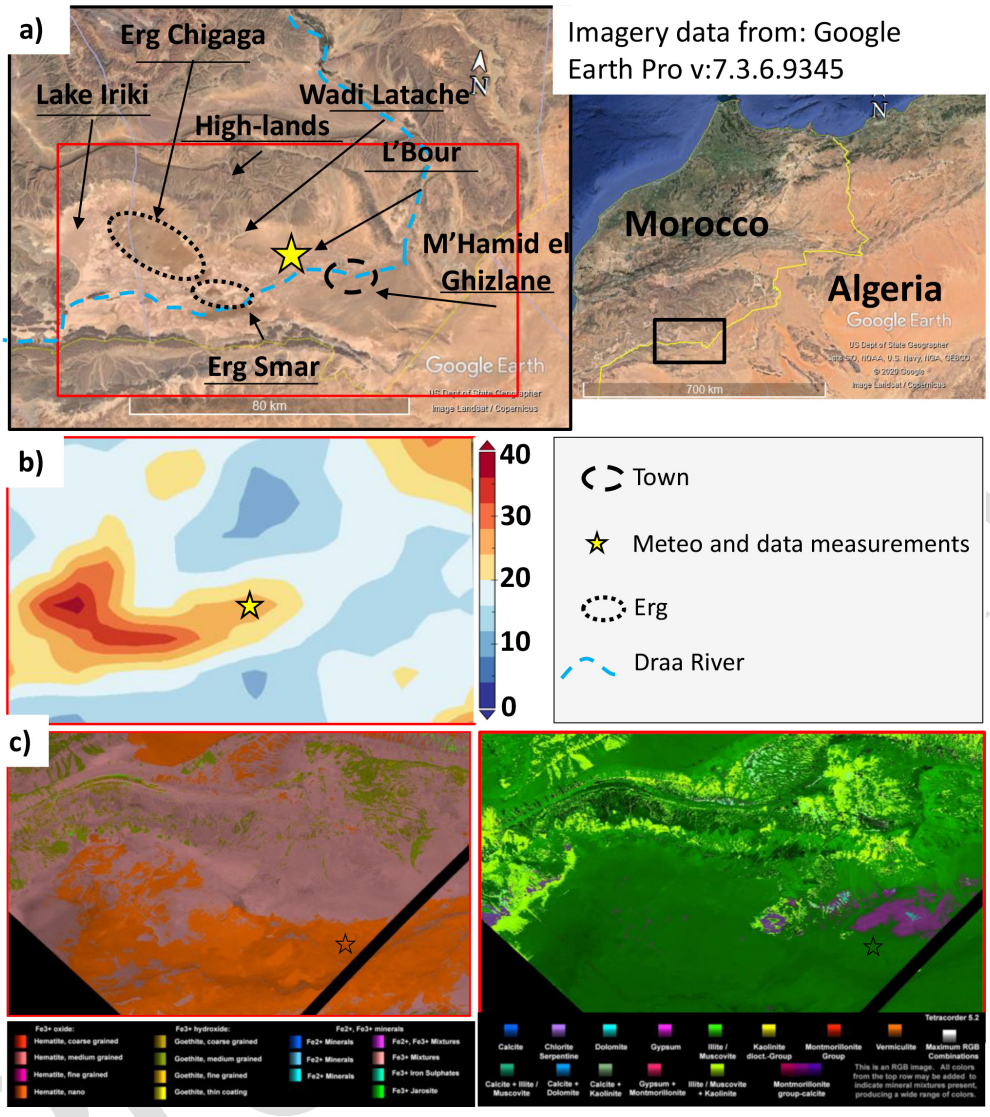

Figure 1. **(a)** Location of the study area (exact location of data measurement "star": 29°49′30″ N, 5°52′25″ W), near M'Hamid el Ghizlane, in the Drâa basin in southern Morocco. Base layer from world imagery of © Google Earth Pro v:7.3.6.9345. **(b)** Frequency of occurrence (%) of dust optical depth above 0.2 in September, October, and November between 2003 and 2016 derived from MODIS Deep Blue. **(c)** EMIT scenes emit20220903t082303_o24606_s001_l2a_rfl_ b0106_v01 and emit20230206t101334_o03707_s000_l2a_rfl_ b0106_v01 at 60 m per pixel show the diversity of Fe^{2+} and Fe^{3+} bearing minerals (left) and the EMIT 8 phyllosilicates, carbonates, and sulfates (right). The mineral maps were produced by tetracorder 5.27c1 (Clark, 2023). There is some mapped mineralogy difference at the scene boundaries, possibly due to the changing viewing geometry, and variation in atmospheric removal between the two scenes. Cirrus clouds in the scene on the right may also be impacting derived mineralogy.

tion of El Mansour Eddahbi dam in 1972 (near Ouarzazate). The Jbel Hassan Brahim range reaches the highest altitude in the area (840 m a.s.l.), while the Drâa River is the lowest point (570 m a.s.l.). The study region corresponds to a low-relief alluvial system, unarmoured and unincised according to Bullard et al. (2011). Rains are scarce, but sometimes they concentrate in the mountains (highlands), and even more sporadically they can directly affect the area during convective storms, creating flash floods with a high sediment load canalised by torrents or wadis, such as Wadi Latache (highlands) (Fig. 1a), which flood flat areas. In specific areas across the basin, highly sediment-loaded waters can be shortly ponded on the way to Drâa River in small depressions, such as dry lake of Lake Iriki, Erg Smar, or L'Bour (lowlands) (Fig. 1a), among other areas, along the floodplain. Dunes are concentrated in small flat areas, near depressions, where, after wind erosion, sediment can be dragged and be entrapped by the very scarce and low vegetation.

2.2 Sediment sampling

The sampled sediments include paleo-sediments (hereafter named sediments), paved sediments, crusts, and dunes, according to the classification by Van der Watt and Valentin (1992) and Valentin and Bresson (1992). Paved sediments result from cyclic drying and aeolian erosion of the surface of paleo-sediments and range from 0.5 to 2 cm of vertical depth. Crusts ranged from 0.1 to 2 cm of vertical depth, and two types are differentiated: (i) thin depositional crusts formed as a result of the deposition of sediments from running water during floods and (ii) thicker sedimentation crusts resulting from the sedimentation and drying of highly sediment-loaded waters in ponded areas of different sizes. The difference between paved sediments and crusts is mostly the period of formation. The former can date up to thousands of years old, while the latter was formed recently. However, crusts might have finer sediments because these are formed by ponding. Sediments are below the crusts (not exposed to the atmosphere), and dunes are aeolian deposits. A 50 cm^2 inox steel shovel was used to sample surfaces (first top centimetre), sediments (below surface, from 1 to 5 cm in the vertical depth), and dunes (from surface to 5 cm). Coordinates, type of sample, surroundings description, and any other important information were registered. A total of 42 sediment samples were obtained, including crusts (12), dunes (12), paved sediments (11), and sediments (7) (Fig. 2), from different locations in the Drâa River basin (Supplement Fig. S1). These were considered representative because the study focuses on sediments (not deposited dust) and one basin.

2.3 Sample treatment

To analyse mineral-size fractionation (< 10 and 10–63 µm), a fully dispersed size fractionation conducted using Milli-Q-grade water and by shaking the samples was applied prior to separation for 12–24 h. First, samples were subjected to 250, 63, and 10 µm sieves to obtain the < 63 and < 10 µm fractions. Due to availability, the smallest opening size of the sieve was 10 µm. Sonic sieving was applied for 60 s at maximum sustainable power for 3 min in every sieve. Finally, subsequent drying at 80 °C was applied to recover the solid fraction from the suspension.

2.4 Analysis

2.4.1 Particle-size distribution and texture

The particle-size analysis was carried out for fully (natural aggregates totally dispersed) and minimally (natural aggregates minimally dispersed) dispersed PSD to obtain the fully dispersed particle-size distribution (FDPSD) and the minimally dispersed particle-size distribution (MDPSD) to evaluate (i) how aggregates and particles occur in natural conditions (MDPSD) and (ii) the distribution of single particles that form the aggregates (FDPSD). The MDPSDs were obtained with laser diffraction using a Malvern Mastersizer 2000 Scirocco accessory (hereinafter Scirocco) for minimally dispersed conditions. In this case, samples of 0.3–0.5 g of the fraction < 2 mm were introduced into the Scirocco vibration plate with a 2 mm aperture and 5 s measuring time. FDPSDs were determined using the Malvern Mastersizer 2000 Hydro G accessory (hereinafter Hydro) with a water suspension and ultrasound assistance for totally dispersed conditions. In that case, the samples were pre-treated following the method by Sperazza et al. (2004). The suspension was introduced into the Hydro's sample container, pumping at 1750 rpm and stirring at 500 rpm. Results were obtained in both cases using the Fraunhofer method (Etzler et al., 1997).

To investigate the possible occurrence of vertical segregation of the PSD (top layers are the ones that are emitting dust), seven crust and five paved sediment samples were selected for vertically resolved PSD analyses. To this end, three sub-samples were extracted from each sample (top, middle, and bottom sections) by scratching the surface with a cutter from top to bottom and were analysed separately. The thickness of these crusts varied between 4 and 8 mm.

The pipette method was also used to analyse the texture of a soil layer or boundary according to FAO-UNESCO (1990) of a total of six samples. This allows us to separate a suspension of the sample in Milli-Q-grade water into different size fractions (> 63, 2–63 and < 2 µm) and dry and analyse each size fraction individually.

2.4.2 Mineralogical composition

Quantitative mineralogical analyses of bulk sediment samples and segregated size fractions were carried out by means of powder X-ray diffraction (XRD), using a Bruker D8 A25 Advance, with Cu $K_{\alpha 1}$ radiation of 1.5405 Å wavelength, Bragg Brentano geometry, and a LynxEyeXE detector. Analysis was performed at 40 mA and 40 kV, with a range of angles from 4 to 60° and angle steps of 0.019° and 10 Hz for 1 h per sample. The mineral identification was done with the EVA software package by Bruker. For quantitative analyses, the method of the internal reference material by Chung (1974) was applied, with quartz as the internal reference. The ratios of intensities of the different minerals versus quartz were obtained by preparing and analysing binary mixtures of the specific minerals and quartz. The accuracy of the XRD quantitative approach was tested by analysing 16 mixtures of reference materials with known concentrations of minerals. Figure S2 summarises major results which yield relative standard deviations versus the known contents of quartz (13 % of error), albite / anorthite (10 %), calcite (31 %), dolomite (14 %), mica / illite (29 %), kaolinite (11 %), gypsum (27 %), anhydrite (19 %), goethite (42 %), and hematite (50 %).

For an in-depth evaluation of clay mineralogy, XRD analyses of oriented aggregates following the procedure by Thorez (1976) were carried out for the same six samples

Proof only

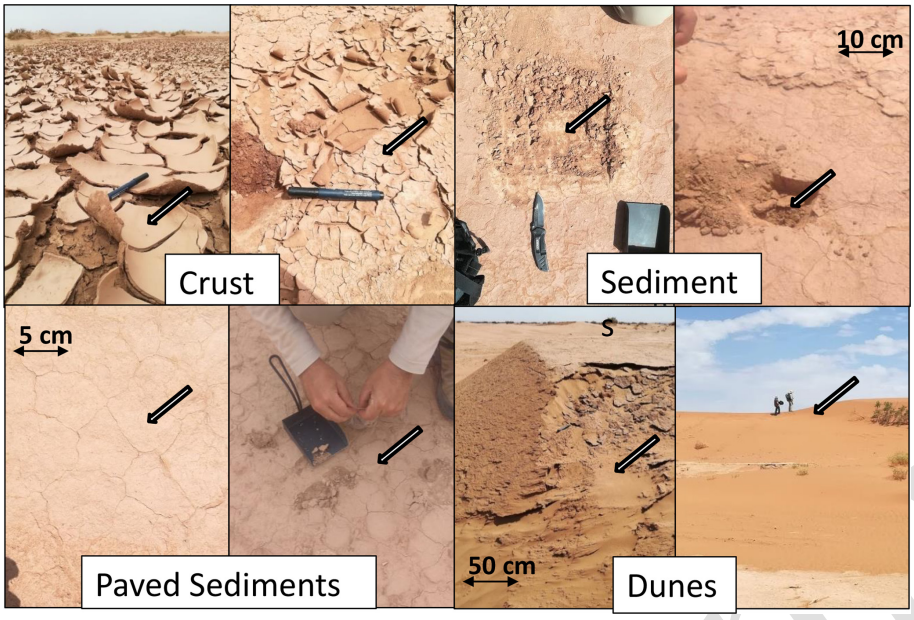

Figure 2. Images of samples collected during a field campaign near M'Hamid el Ghizlane, into the Drâa River basin, southern Morocco.

of the texture. The samples were treated for air drying (AO), glycolation (AG), and heating (AC). Mica / illite, chlorite / kaolinite, palygorskite, and smectite were found in all the samples, as evidenced from the bulk XRD analysis. Calcite and dolomite were dissolved by acidifying soil suspension with a strong acid as HCl and the excess also used to stoichiometrically quantify the content of carbonates using the method proposed by Horváth et al. (2005) for the same six samples of the clay-oriented aggregates and texture.

To investigate the possible occurrence of mineralogical vertical segregation, the seven crust and five paved sediment unaltered samples used for particle-size analysis (see Sect. 2.4.1) were also used for vertically resolved mineralogy analyses.

2.4.3 Mode of occurrence of Fe

Fe is a key ingredient to climatic and biological processes affected by dust. For instance, the amount, mixing state, and size of Fe-oxy/hydroxides determine the degree of absorption of solar radiation by dust (Engelbrecht et al., 2016) and the potential solubility of the dust deposited into the ocean (Shi et al., 2012). However, the XRD semiquantitative analysis for Fe-oxy/hydroxides is affected by large uncertainties due to the low concentrations (increasing relative errors) and is not sensitive to nano-Fe oxides (Shi et al., 2012). XRD analyses were complemented by quantifying the levels and mode of occurrence of Fe in the bulk samples, as described in Shi et al. (2009). The method is based on a sequential extraction protocol to obtain the proportions of readily exchangeable (adsorbed) Fe ions and Fe in nano-Fe oxides (FeA) and the amount of Fe in crystalline Fe oxides, mainly from hematite and goethite (FeD) in the samples. A quantity of 30 mg of Arizona Test Dust (ATD; ISO 12103-1, A1 Ultrafine Test Dust; Powder Technology Inc.) was used to test the accuracy of the method, and extractions were done with 15 mL of extractant solution. For total Fe content (FeT), a two-step wet-acid-digestion method developed by Querol et al. (1993, 1997) and a coal fly ash (1633b) standard sample were used to test accuracy. The 1633b gave 7.5 % with a standard deviation of 0.14 % for total Fe (reference content of 7.8 % of Fe), while ATD gave 0.076 % with a standard deviation of 0.002 % of FeA and 0.49 % with a standard deviation of 0.07 % for FeD + FeA (reference content of 0.067 % of FeA and 0.41 % of FeD). Furthermore, by subtraction, the contents of structural Fe (FeS = FeT − (FeA + FeD)) were obtained, corresponding to the Fe fraction as elemental Fe into the structure of minerals other than Fe oxides, such as illite or other Fe-bearing minerals. Furthermore, the FeD contents were converted stoichiometrically to hematite (Fe_2O_3) and goethite (FeO(OH)) using the hematite / goethite proportions from XRD.

2.4.4 Electron microscopy of crust and paved sediment sections

The PSD, mineralogy and morphology of crust and paved sediments can vary along the vertical profile, especially in crusts where progressive sedimentation and subsequent evaporation lead to inter-layering of sediments with different properties. For that purpose, crust and paved sediment sections were impregnated with epoxy resin, cut, and polished with diamond paste for microscopy analysis. The polished samples were coated with graphite before analysis with a

Proof only

JEOM JSM-7001F SEM-EDX scanning electron microscope (SEM).

3 Results and discussion

3.1 Regional variability

3.1.1 Particle-size distribution

The PSDs of the samples collected across the basin were analysed to detect possible trends or size segregation patterns from high- to lowlands for the different types of sediment. The mean median diameter values of each group of sediments provided in this section represent the mean and standard deviation of the median diameters. Because the PSDs are generally bimodal, other PSD metrics can be found in Table 1, including the maximum, minimum, and mean of the median diameters for different types of sediments, location, PSD type (MDPSD and FDPS), and size fraction (full range, < 63 and > 63 to < 2000 µm).

MDPSDs, excluding dune samples, show a major mode centred around 100 µm in diameter and a secondary one between 2 and 20 µm (Fig. 3a; Table 1). FDPSDs also show two modes at 5 and 100 µm (Fig. 3b; Table 1). The MDPSDs and FDPSDs of dune samples are very similar, with a main mode centred around 150 µm and a secondary small one at 5 µm (30 times lower) (Fig. 3c and d). Crust samples show the largest fine (0–5 µm) fraction in MDPSD, followed by paved sediments and sediments (Fig. 3e). FDPSDs show a similar trend but with a larger proportion of fine particles compared to MDPSD (Fig. 3f).

The mean median diameter of the MDPSDs (Fig. 4a), excluding dune samples, is 88 ± 63 µm; and that of the FDPSDs is 27 ± 51 µm (Fig. 4a). Therefore, aggregates are about 3 times coarser than individual mineral particles. As expected, dunes were coarser than other types of sediments, with a mean median diameter of 219 ± 70 µm of the FDPSDs, which is very similar to that of the MDPSDs (Fig. 4b). The mean median diameters of MDPSDs are 70 ± 48, 74 ± 45 and 113 ± 79 µm for sediments, paved sediments, and crusts, respectively (Fig. 4c), whereas the mean diameters of FDPSDs are 19 ± 11, 21 ± 26, and 37 ± 77 µm for sediments, paved sediments, and crusts respectively, about 3 to 4 times finer (Fig. 4d).

The spatial variation of the mean diameter of the FDPSDs (Fig. 5) shows coarser crusts (> 40 µm) close to the highland areas and finer crusts (< 40 µm) near the Drâa River, likely due to flooding (causing transport and deposition of fine sediments, especially in the lowlands) caused during scarce and intensive rains. For paved sediments, sediments, and dunes, spatial PSD trends were not evident, with mean median diameters ranging from 10 to 120, 10 to 40, and 120 to 300 µm, respectively, randomly located across the basin (Table 1).

According to the size classification by Valentin and Bresson (1992), and using the FDPSD data (Fig. S3), dune samples can be classified as sand, loamy sand, and sandy loam; sediments as silt loam and loam; paved sediments as sandy loam, loam, and silt loam; and crusts as sandy loam, loam, silty clay loam, and silt loam. As shown in Fig. S3 and due the higher transport potential of clays during rain episodes, and their accumulation during ponding, crusts tend to be further enriched in clay fractions, especially in lowlands, compared to paved sediments and sediment samples (see Sect. 3.4).

3.1.2 Mineralogical composition

Here the mineralogy of samples collected across the basin is described to detect possible trends or mineral segregation patterns from high- to lowlands for the different types of sediment. The mineralogical composition (mass % composition of the bulk sample) of dunes, crusts, paved sediments, and sediment samples is summarised in Table 2. Dunes show a homogeneous mineralogy across the study area, with mineral abundances of 74 ± 9.7 % quartz, 5.8 ± 2.9 % calcite, 6.7 ± 3.6 % microcline, 6.9 ± 3.1 % albite / anorthite, 4.1 ± 2.3 % clay minerals, 1.0 ± 1.4 % dolomite, 0.38 ± 0.26 % goethite and 0.12 ± 0.11 % hematite and trace amounts of halite and gypsum (< 0.1 %) (Fig. 6). In comparison to dunes, crusts are depleted in quartz (48 ± 11 %) and feldspars (5.0 ± 2.1 % albite / anorthite and 4.4 ± 3.1 % microcline) and enriched in clay minerals (17 ± 8.0 %), calcite (19 ± 8.0 %), dolomite (3.0 ± 1.3 %), and Fe oxides (0.24 ± 0.28 % hematite and 0.42 ± 0.56 % goethite) (Fig. 6). The content of gypsum (0.23 ± 0.56 %) and halite (2.9 ± 5.1 %) is higher than in dune samples, but variability is large because it depends on the exact point of crust sampling. Paved sediments have a similar mineralogy than crusts, for quartz (51 ± 8.7 %), calcite (17 ± 4.9 %), clay minerals (16 ± 7.3 %), albite / anorthite (6.3 ± 1.8 %), microcline (4.5 ± 2.5 %), dolomite (3.5 ± 0.79 %), hematite (0.34 ± 0.25 %), and goethite (0.38 ± 0.38 %) but with lower content of gypsum (< 0.1 %) (Fig. 6). Sediments are also similar to paved sediments and crusts with a mean quartz content (55 ± 11 %), calcite (17 ± 4.6 %), clay minerals (14 ± 6.8 %), albite / anorthite (5.8 ± 1.5 %), microcline (3.7 ± 1.6 %), dolomite (3.4 ± 1.3 %), hematite (0.28 ± 0.37 %), and goethite (0.37 ± 0.32 %). Trace amounts of gypsum (< 0.1 %) and halite (0.32 ± 0.55 %) were also found in sediments (Fig. 6).

In comparison with the bulk sediment, the fully dispersed silt fraction (10–63 µm) shows a lower amount of quartz (35 ± 6.4 %) and feldspars (7.4 ± 2.5 %); a higher content of carbonates (25 ± 5.2 %), clays (22 ± 10 %), and hematite (1.07 ± 0.38 %); and a similar content of goethite (0.61 ± 0.32 %). In the fully dispersed < 10 µm sieved fraction, the amount of quartz (23 ± 5.2 %) and feldspars (4.7 ± 1.1 %) is 2 times lower than in the bulk sediments. The fraction of carbonates remains similar (21 ± 9.0 %), and the content of clays increases substantially (38 ± 9.8 %) com-

Proof only

Table 1. Full range, < 63 µm and > 63 to 2000 µm mean diameter, standard deviation, and min and max for minimally dispersed particle-size distribution and fully dispersed particle-size distribution. NaN: not a number.

Surface type	Location	Number of samples	MDPSD		
			Full range	≤ 63 µm	> 63 to 2000 µm
			Mean of medians ± SD [min, max]		
Dunes	Mean	12	221 ± 64 [132, 355]	32 ± 9.3 [20, 46]	252 ± 65 [142, 364]
	Highland	3	212 ± 27 [195, 243]	45 ± 1.3 [44, 46]	259 ± 22 [243, 284]
	Erg Smar	4	286 ± 49 [244, 355]	32 ± 8.1 [25, 41]	295 ± 52 [238, 364]
	L'Bour	5	174 ± 45 [132, 244	27 ± 7.4 [20, 36]	214 ± 76 [142, 332]
Crusts	Mean	12	113 ± 79 [20, 320]	15 ± 3.7 [7.7, 19]	308 ± 146 [146, 635]
	Highland	3	94 ± 5 [89, 99]	18 ± 1.1 [17, 19]	219 ± 28 [187, 238]
	Erg Smar	8	131 ± 89 [21, 320]	13 ± 3.4 [7.7, 17]	362 ± 151 [193, 635]
	L'Bour	1	20 ± NaN [NaN, NaN]	15 ± NaN [NaN, NaN]	146 ± NaN [NaN, NaN]
Paved sediments	Mean	11	74 ± 48 [19, 152]	17 ± 6.7 [11, 33]	237 ± 71 [146, 387]
	Highland	0	NaN	NaN	NaN
	Erg Smar	8	68 ± 46 [19, 148]	17 ± 7.0 [11, 33]	240 ± 43 [167, 320]
	L'Bour	3	90 ± 61 [29, 148]	18 ± 7.1 [13, 26]	230 ± 137 [146, 387]
Sediments	Mean	7	70 ± 45 [20, 147]	18 ± 5.1 [15, 29]	175 ± 58 [129, 302]
	Highland	1	97 ± NaN [NaN, NaN]	18 ± NaN [NaN, NaN]	149 ± NaN [NaN, NaN]
	Erg Smar	2	115 ± 45 [83, 147]	22 ± 11 [15, 29]	229 ± 104 [155, 302]
	L'Bour	4	40 ± 23 [20, 68]	17 ± 0.79 [16, 17]	155 ± 21 [129, 178]
				FDPSD	
Dunes	Mean	12	219 ± 70 [128, 312]	24 ± 13 [9.0, 46]	247 ± 72 [145, 355]
	Highland	3	250 ± 73 [169, 312]	41 ± 6.8 [33, 46]	290 ± 77 [205, 355]
	Erg Smar	4	263 ± 32 [239, 308]	20 ± 6.2 [13, 25]	279 ± 33 [238, 319]
	L'Bour	5	166 ± 61 [128, 272]	16 ± 7.5 [9.0, 26]	195 ± 68 [145, 310]
Crusts	Mean	12	37 ± 77 [2.7, 272]	9.8 ± 3.6 [3.6, 16]	196 ± 76 [119, 389]
	Highland	3	124 ± 132 [20, 272]	13 ± 1.1 [12, 14]	251 ± 121 [162, 389]
	Erg Smar	8	7 ± 3 [2.7, 10]	7.9 ± 2.5 [3.6, 11]	183 ± 44 [130, 236]
	L'Bour	1	17 ± NaN [NaN, NaN]	16 ± NaN [NaN, NaN]	119 ± NaN [NaN, NaN]
Paved sediments	Mean	11	21 ± 26 [2.3, 78]	13 ± 4.8 [8.2, 21]	157 ± 36 [120, 221]
	Highland	0	NaN	NaN	NaN
	Erg Smar	8	18 ± 24 [5.9, 78]	12 ± 4.6 [8.2, 21]	169 ± 34 [129, 221]
	L'Bour	3	29 ± 33 [5.3, 67]	14 ± 6.0 [8.3, 20]	122 ± 2.2 [120, 124]
Sediments	Mean	7	19 ± 11 [5.8, 39]	14 ± 3.9 [7.7, 19]	128 ± 9.6 [117, 144]
	Highland	1	12 ± NaN [NaN, NaN]	9.9 ± NaN [NaN, NaN]	133 ± NaN [NaN, NaN]
	Erg Smar	2	22 ± 23 [5.8, 39]	13 ± 8.1 [7.7, 19]	126 ± 13 [117, 135]
	L'Bour	4	19 ± 6.3 [13, 28]	15 ± 1.3 [13, 17]	128 ± 11 [122, 144]

Proof only

pared to the bulk and silt-size mineralogy. The Fe oxide content increases by about a factor of 2 for both hematite (2.2 ± 2.0 %) and goethite (1.8 ± 1.2 %). Table 3 compares the mineralogical results in the clay and silt size ranges, both with the fully dispersed separation and the pipette methods, against the corresponding values provided by the available global mineralogical atlases of Claquin et al. (1999) and Journet et al. (2014), which assume the sample locations to be either Fluvisols or Yermosols in terms of soil type. In the silt-size fraction, similar contents of quartz, total clay, mica / illite, chlorite + kaolinite, calcite, and Fe oxides were found but 3 times less feldspar and 5 times more dolomite. Compared to the clay-size fraction in the atlases, the < 10 µm fraction in this study shows larger content of quartz and feldspars (by a factor of 2 to 4), a 30 % lower total clay content, and similar contents of calcite and Fe oxides, which can only be partly explained by the difference in the size fraction considered (< 10 µm vs. < 2 µm) as shown by the results obtained with the pipette method. Because kaolinite and chlorite have coincident spacing at 7 Å in the XRD spectra, in current atlases these minerals may be confounded, whereas in this study chlorite was quantified separately by identifying other minor peaks in the spectra. This is relevant as both minerals are very different in terms of chemical

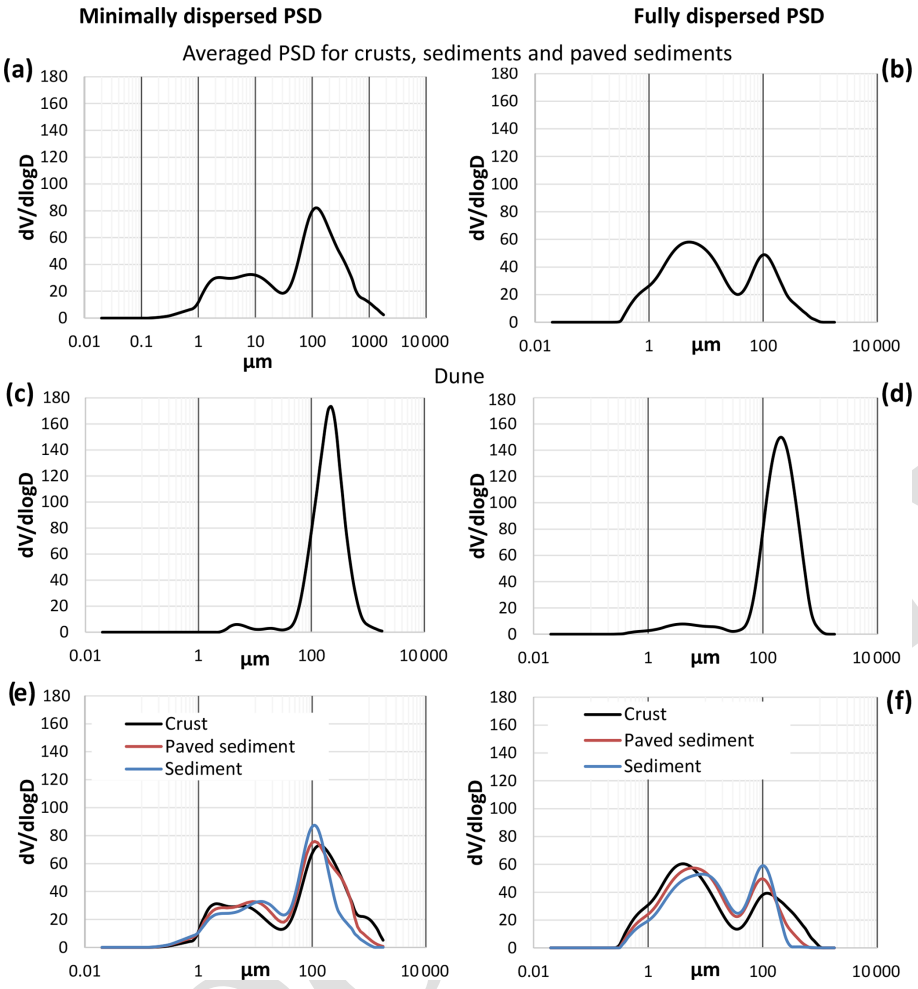

Figure 3. Median minimally and fully dispersed PSDs of crusts, sediments, paved sediments, and dunes. **(a)** MDPSDs and **(b)** FDPSDs are combined from crust, sediment, and paved sediment samples; **(c)** and **(d)** are MDPSDs and FDPSDs for dune samples; and **(e)** and **(f)** are MDPSDs and FDPSDs differentiated by type of sample.

composition. In this study, minor concentrations of dolomite and traces of smectite and palygorskite were also detected. The large differences in the silt-size feldspar content may be largely due to the lack of data and coarse assumptions used in current atlases.

Table S1 in the Supplement compares the silt+clay and sand proportions and the mineral contents of the crusts from this study in Morocco with those from deposited dust in different arid regions of the world. The FD-PSD data from this study evidence that 72 % of the particles in the crusts fall in the clay + silt fraction (< 63 µm), while 28 % fall in the sand size range. This is close to the average value (74 % and 26 %, respectively) calculated from the existing studies on deposited dust. Concerning the mineralogy, the crusts of this study are enriched in clays and depleted in carbonate minerals and feldspars compared with the average of the mineralogy of deposited dust (Table S1).

In this analysis of trends in mineralogy from the highlands to the lowlands, all sample types, except dunes, were considered. The lowlands, such as L'Bour and Erg Smar, are enriched in clay minerals (17 ± 9.6 % and 14 ± 3.4 %, respectively) compared to the highlands (9.1 ± 0.97 %) (Fig. 6). Mica / illite is the most common clay mineral reaching mean contents of 9.1 ± 4.8 % and 8.1 ± 2.0 % in Erg Smar and L'Bour, respectively, and 5.0 ± 0.70 % in the highlands. Kaolinite reaches 7.2 ± 5.4, 4.9 ± 2.1 %, and 3.5 ± 0.30 % and clinochlore 1.7 ± 1.8 %, 1.3 ± 0.67 %, and 0.49 ± 0.38 %, respectively. Smectite and palygorskite were detected only in trace amounts (< 0.1 %) in most samples, with only palygorskite at Erg Smar and in the highlands reaching a mean content of $0.34 \pm 0.58\,0.06$ % and 0.15 ± 0.06 %, respectively. The same trend is found for calcite (24 ± 13 %, 16 ± 3.1 %, and 11 ± 2.7 % at Erg Smar and L'Bour and in the highlands), dolomite (5.0 ± 5.1 %, 3.6 ± 0.51 %, and 1.7 ± 0.50 %, at Erg Smar and L'Bour

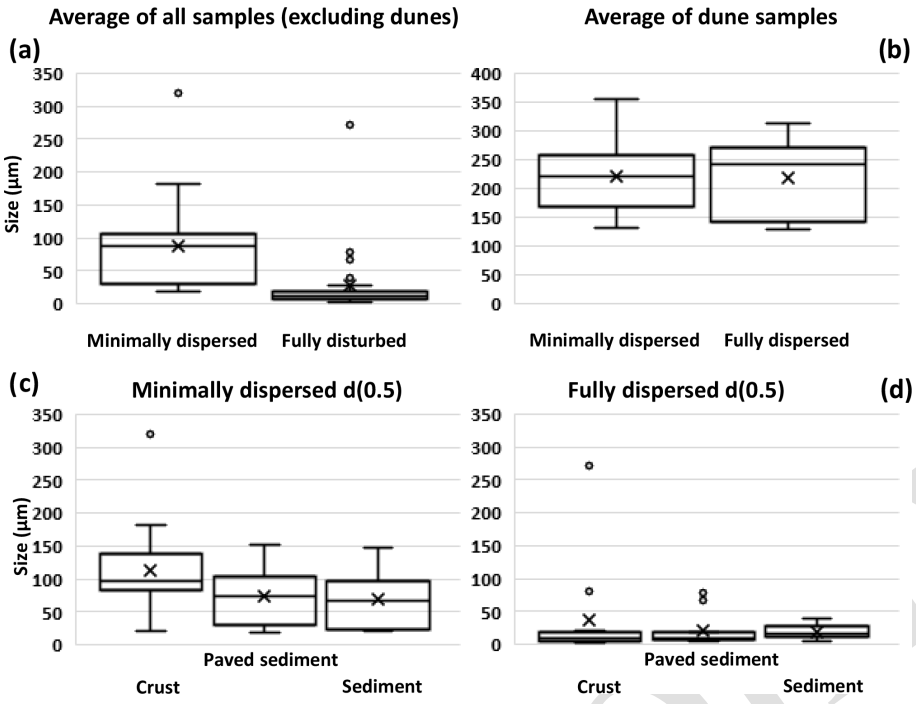

Figure 4. Box plot of median particle-size diameters (in µm) including both fully and minimally dispersed analysis **(a)** for all samples combined excluding dunes and **(b)** for dune samples only. Also particle-size diameter (in µm) for crusts, sediment, and paved sediment for **(c)** minimally dispersed and **(d)** fully dispersed results. Mean median diameters for each sediment type are shown with crosses.

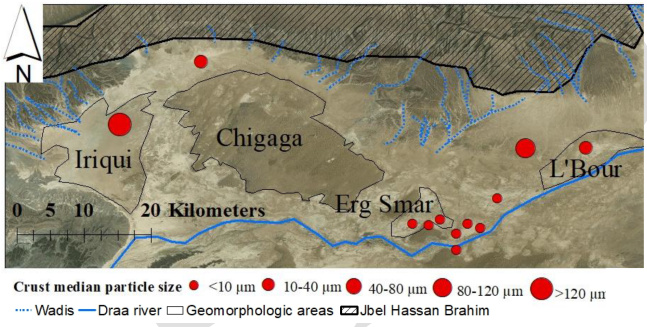

Figure 5. Spatial variation map with crust fully dispersed mean median particle diameter.

and in the highlands), and Fe oxides (0.78 ± 1.4 %, 0.37 ± 0.43 %, and 0.08 ± 0.04 % for hematite at Erg Smar and L'Bour and in the highlands and 0.42 ± 0.51 %, 0.39 ± 0.35 %, and 0.32 ± 0.21 % for goethite at Erg Smar and L'Bour and in the highlands), which is steeper for hematite than goethite (Fig. 6). Quartz follows an opposite trend, increasing towards the highlands (42 ± 18 %, 53 ± 5.0 %, and 61 ± 5.4 %, at Erg Smar and L'Bour and in the highlands, respectively) (Fig. 6). Albite / anorthite and microcline do not show a clear trend, with 5.5 ± 2.3 %, 5.9 ± 1.8 %, and 5.4 ± 1.2 % at Erg Smar and L'Bour and in the highlands and 3.4 ± 2.4 %, 5.0 ± 3.4 %, and 4.6 ± 1.7 %, respectively (Fig. 6). Salt concentrations peak randomly and depend on very local-scale conditions, being higher at concave areas where ponding is favoured (see Sect. 3.4). The mean content of halite is 1.0 ± 2.2 %, < 0.1 %, and 4.0 ± 7.7 % at Erg Smar and L'Bour and in the highlands, and that of gypsum is 0.18 ± 0.35 %, < 0.1 %, and 0.15 ± 0.92 %, respectively (Fig. 6).

A soft crust occurred on the surface of several dunes (Fig. 2). The PSD and mineralogical analysis of the crust and the underlying sands did not reveal significant differences. Pye and Tsoar (2015) reported that surface hardening of dunes is due to the scavenging and deposition of clays from suspended dust in light rains and by cementation of sand particles (meniscus) by precipitation of carbonates and silica in the retained interstitial pore water. In both cases the potential variability caused by the slight increase in this clay and carbonate / silica cementation is obscured by variations in the bulk mineralogy.

3.2 Vertical segregation in crust and paved sediments

The examination of thin vertical cross-sections provides insight into how particle size and mineral composition vary within the top few micrometres or millimetres of the surface. These differences are relevant to the mineralogy and PSD of newly emitted dust.

Table 2. Mineral results from samples and type of sample. In type of samples, C: crust, PS: paved sediment, S: sediment, and D: dune. In Loc (location), ES: Erg Smar, LB: L'Bour, HL: highlands. Sme: smectite, Mca: mica/illite, Kln: kaolinite, Chl: chlorite, Plg: palygorskite, Qtz: quartz, Cal: calcite, Dol: dolomite, Hl: halite, Gp: gypsum, Mc: microcline, Ab: albite and anorthite, Hem: hematite, and Gt: goethite. <0.1 indicates below the limit of detection.

		Feldspars			Carbonates		Clays					Salts		Iron oxides	
Type	Loc	Qtz	Mc	Ab	Cal	Dol	Sme	Mca	Kln	Chl	Plg	Hl	Gp	Hem	Gt
C	ES	55	2.6	4.8	20	3,3	<0.1	11	<0.1	1.2	<0.1	<0.1	<0.1	1.2	<0.1
C	ES	57	2.7	3.1	20	3.4	<0.1	5.2	<0.1	0.78	0.26	7.2	<0.1	0.87	<0.1
C	ES	36	2.2	10	21	2.7	<0.1	15	10.0	1.4	<0.1	<0.1	0.20	1.2	<0.1
C	ES	32	1.7	3.3	29	3.4	<0.1	10	17	2.2	0.20	<0.1	<0.1	0.24	1.3
C	ES	38	3.7	4.7	18	6.2	<0.1	14	9.0	1.3	0.14	3.5	0.14	0.95	<0.1
C	ES	50	5.5	5.5	14	2.8	<0.1	12	7.9	1.3	<0.1	<0.1	<0.1	0.21	0.85
C	LB	50	13	5.1	12	3.6	<0.1	8.1	5.7	0.46	<0.1	<0.1	<0.1	0.92	<0.1
C	HL	63	6.9	6.8	12	2.2	<0.1	4.5	3.9	0.19	<0.1	<0.1	<0.1	0.11	0.40
C	ES	45	3.7	3.2	26	3.2	<0.1	11	5.4	1.8	0.21	<0.1	<0.1	<0.1	0.18
C	ES	30	2.6	3,4	35	2.5	0.57	8.8	14	1.4	1.5	0.14	<0.1	0.14	0.17
C	HL	60	3.7	5.5	11	0.98	<0.1	5.7	3.4	0.97	0.19	8.1	0.21	0.41	0.60
C	HL	54	4.7	3.9	7.1	1.79	<0.1	5.4	3.3	0.60	<0.1	16	2.0	0.22	0.65
S	ES	35	1.8	4.1	24	5.6	<0.1	17	8.3	2.2	<0.1	1.1	0.19	1.1	<0.1
S	ES	67	6.6	5.1	10	2.1	<0.1	3.0	3.6	0.64	<0.1	1.1	<0.1	0.42	0.23
S	LB	51	4.6	7.9	15	4.2	<0.1	8.9	6.6	0.89	<0.1	<0.1	<0.1	<0.1	0.82
S	LB	57	2.7	7.8	16	3.8	<0.1	9.6	1.9	0.49	<0.1	<0.1	<0.1	0.93	<0.1
S	LB	57	3.4	5.4	18	3.2	<0.1	6.5	3.5	2.1	<0.1	<0.1	<0.1	0.33	0.60
S	HL	67	3.2	5.3	13	1.7	0.13	4.3	3.2	0.20	0.20	<0.1	<0.1	<0.1	0.90
S	LB	51	3.4	5.1	21	3.3	<0.1	8.5	4.5	2.2	0.15	<0.1	<0.1	0.66	0.50
PS	ES	44	3.0	5.7	15	3.1	<0.1	16	11	1.5	<0.1	<0.1	<0.1	0.35	0.64
PS	ES	44	2.2	5.4	22	4.7	<0.1	13	6.8	0.54	<0.1	<0.1	<0.1	1.1	<0.1
PS	ES	55	2.3	5.4	24	3.6	<0.1	7.8	0.84	0.28	0.17	<0.1	<0.1	0.98	<0.1
PS	ES	40	5.3	4.7	20	4.3	<0.1	13	10	1.1	<0.1	<0.1	0.29	0.77	0.23
PS	ES	67	8.8	8.7	8.9	1.8	<0.1	3.1	0.38	0.30	<0.1	<0.1	<0.1	0.30	0.29
PS	LB	48	5.5	4.0	16	4.3	<0.1	11	8.7	1.3	0.13	<0.1	<0.1	1.1	<0.1
PS	ES	61	3.5	6.3	12	3.6	<0.1	7.9	3.6	0.78	0.16	<0.1	<0.1	0.41	0.33
PS	ES	46	9.1	9.0	14	3.3	0.29	6.6	8.8	1.0	0.42	<0.1	<0.1	0.42	0.69
PS	ES	48	2.3	7.3	22	3.7	<0.1	8.1	6.3	1.3	<0.1	<0.1	0.16	0.17	1.1
PS	LB	61	4.0	8.1	13	3.3	<0.1	4.3	4.2	1.2	<0.1	<0.1	<0.1	0.16	0.64
PS	LB	51	3.6	4.4	22	3.1	<0.1	8.5	4.3	2.0	0.17	<0.1	<0.1	0.68	0.53
D	ES	80	7.1	7.0	3.1	0.69	<0.1	1.4	<0.1	<0.1	<0.1	<0.1	<0.1	<0.1	0.38
D	ES	65	14	8.3	4.1	0.90	<0.1	4.8	1.9	<0.1	<0.1	<0.1	<0.1	<0.1	0.37
D	LB	73	7.0	11	6.6	0.31	<0.1	1.2	0.19	0.23	<0.1	<0.1	<0.1	0.11	0.32
D	ES	89	2.5	3.0	2.0	<0.1	<0.1	0.69	1.4	<0.1	<0.1	<0.1	<0.1	0.45	0.65
D	ES	65	12	5.4	11	1.3	0.13	2.7	2.1	0.38	<0.1	<0.1	<0.1	0.12	0.32
D	LB	64	5.0	6.8	10	5.0	<0.1	3.1	4.3	0.50	<0.1	<0.1	<0.1	<0.1	0.61
D	LB	76	4.1	6.7	6.6	0.52	<0.1	2.6	2.2	0.21	<0.1	0.28	<0.1	0.25	0.21
D	LB	77	3.9	6.7	7.5	0.53	0.26	1.5	1.6	0.49	<0.1	0.34	<0.1	0.13	0.50
D	LB	57	11	14	7.5	1.8	<0.1	3.4	3.0	0.74	<0.1	<0.1	<0.1	0.16	0.37
D	HL	85	4.8	4.0	3.7	0.33	<0.1	1.1	0.22	0.51	<0.1	<0.1	<0.1	<0.1	0.69
D	HL	82	9.2	3.3	2.8	0.17	0.15	1.2	0.67	<0.1	<0.1	<0.1	<0.1	0.20	0.29
D	HL	77	6.9	7.3	4.5	0.34	<0.1	1.7	1.3	0.39	<0.1	<0.1	<0.1	<0.1	0.41

The MDPSDs of crust sections (top, middle and bottom) are very similar, with two modes of occurrence at 5–7 and 200 µm (Fig. S4a). Yet, while the FDPSDs show two similar modes at 1–5 and 100 µm for the top and middle sections and a second mode at 300 µm for the bottom section (Fig. S4b). The MDPSD mean median diameter of the seven crust profiles reaches 25 ± 25, 54 ± 80, and 25 ± 26 µm for the top, middle, and bottom sections, respectively, while FDPSD means are 9.4 ± 9.4 and 11 ± 9.5 µm in the top and middle sections and 94 ± 145 µm in the bottom one (Fig. S4c and

Proof Only

Table 3. Mineralogy of specific soils according to Claquin et al. (1999) and Journet et al. (2014) and comparison with the one obtained in this study for six selected samples. Bulk, clay, and silt fractions' mineralogy (obtained from texture fractionation) and $< 10\,\mu m$ and silt (10–63 µm) fractions' mineralogy using fully dispersed separation. All content is in mass percent. NaN: not a number.

			Carbonates		Clays						Salts		Fe oxides	
	Qtz	Feld	Cal	Dol	Mca	Chl	Sme	Plg	Kln	Tot.clay	Gp	Hal	Hem	Gt
Bulk	58	9.5	15	2.4	6.4	1.0	0.1	0.2	3.8	11	0.2	8.1	0.5	0.5
Clay Ye Claquin	5	NaN	6	NaN	89	NaN	NaN	NaN	NaN	≈ 89	NaN	NaN	NaN	NaN
Clay Ye Journet	8	3	18	NaN	67	NaN	NaN	1	3	≈ 71	NaN	NaN	NaN	NaN
Clay Fl Claquin	12	NaN	11	NaN	77	NaN	NaN	NaN	NaN	≈ 77	NaN	NaN	NaN	NaN
Clay Fl Journet	NaN	NaN	NaN	NaN	98	NaN	NaN	1	1	≈ 100	NaN	NaN	NaN	NaN
Clay classic Drâa	17	7.1	8.9	0.5	23	9.9	1.2	1.0	22	57	NaN	NaN	0.7	5.2
$< 10\,\mu m$ FD Drâa	23	4.7	19	2.4	19	4.7	0.4	0.2	14	38	NaN	NaN	2.2	1.8
Silt Ye Claquin	58	31	8	NaN	NaN	NaN	NaN	NaN	NaN	NaN	2	NaN	1	NaN
Silt Ye Journet	43	21	20	NaN	9	6	NaN	NaN	NaN	15	NaN	NaN	1	NaN
Silt Fl Claquin	30	38	29	NaN	NaN	NaN	NaN	NaN	NaN	NaN	2	NaN	NaN	NaN
Silt Fl Journet	39	19	12	NaN	19	10	NaN	NaN	NaN	29	NaN	NaN	1	NaN
Silt classic Drâa	30	8	12	4.9	19	6.4	0.3	0.1	13	39	NaN	NaN	0.2	0.6
Silt FD Drâa	39	8.0	23	5.0	12	2.8	0.2	< 0.1	7.5	23	NaN	NaN	1.2	0.7

Fl: Fluvisol sediment type, Ye: Yermosol, Qtz: quartz, Feld: feldspars, Cal: calcite, Dol: dolomite, Mca: mica / illite, Chl: chlorite, Sme: smectite, Plg: palygorskite, Kln: kaolinite, Gp: gypsum, Hal: halite, Hem: hematite, Gt: goethite, and FD: fully dispersed.

d). Therefore, during the initial stages of ponding, coarser particles are deposited first, while finer particles remain suspended (see Sect. 3.4) in the later stages before evaporation of the water. Even some oxides, carbonates, and salts may precipitate in the top layers of the crust as water evaporates and the ionic strength increases.

No vertical PSD segregation is observed in paved sediments, but some top sections analysed show enrichment in coarser fractions in FDPSD (the median diameter increases from bottom and middle sections (14 ± 6.8 and $12 \pm 5.8\,\mu m$) to the top section ($23 \pm 28\,\mu m$)), likely due to preferential erosion of finer fractions through sandblasting (see Sect. 3.4).

The mean levels of quartz and feldspars are enriched in the bottom sections of the crusts (46 ± 17 % and 8.7 ± 4.6 %, respectively) compared to the middle (38 ± 11 % and 8.3 ± 2.5 %) and top sections (41 ± 12 % and 6.9 ± 2.2 %) due to the higher quartz content of the coarse fraction that is deposited first (see Sect. 3.4). The content of clay minerals, salts, and Fe oxides is similar in the top (20 ± 7.2 %, < 0.1 % and 3.3 ± 1.9 %, respectively), middle (21 ± 5.0 %, < 0.1 % and 2.8 ± 1.6 %), and bottom sections (19 ± 9.1 %, < 0.1 % and 1.9 ± 1.0 %). Carbonate minerals are relatively homogeneous but slightly enriched in the middle and top sections (29 ± 9.7 % and 28 ± 7.9 %, respectively) compared to the bottom section (24 ± 8.4 %). This can arise from both detrital carbonate particles and precipitation from high-ionic-strength waters that are ponded and dried in the lowlands.

The mineral composition of the paved sediment profiles differs slightly from that of crust profiles. This is because the latter are affected by particle segregation during transport and subsequent sedimentation. The top section of the paved sediment profiles has more quartz than in the middle and bottom sections (44 ± 8.1 %, 38 ± 5.7 % and 40 ± 9.8 %, respectively), whereas feldspars decrease from the bottom and middle to the top sections (9.1 ± 4.2 %, 9.3 ± 2.2 %, and 6.9 ± 2.7 %). Carbonates and clay are relatively homogeneous (26 ± 4.9 %, 26 ± 2.0 %, and 25 ± 4.2 % for carbonates and 22 ± 8.4 %, 23 ± 9.2 %, and 25 ± 4.9 % for clays, respectively). The slight depletion of minerals in the top section may be due to sandblasting, which tends to erode the fine fraction of the surface over time (see Sect. 3.4). Fe oxides are more present in the top section than in the middle and bottom sections (2.1 ± 0.47 %, 2.0 ± 0.38 % and 1.7 ± 0.27 %, respectively), and the presence of salts is very low (< 0.1 % for all sections).

3.3 Mode of occurrence of Fe

A sequential Fe extraction procedure was implemented to evaluate the levels and mode of occurrence of Fe in dust samples from the basin. Due to limitations of XRD analysis for low-Fe-oxide contents, this procedure provided a much more precise quantitative evaluation.

The mean FeT content of bulk crusts, paved sediments, and sediments was found to be 3.6 ± 0.71 %, 3.4 ± 0.47 %, and 3.2 ± 0.44 %, respectively, while bulk dunes had a much lower FeT content (2.0 ± 0.33 %). Fe-speciation studies reveal that the FeS percentage from FeT (FeS / FeT) is the prevailing Fe mode of occurrence (67 ± 2.4 %, 69 ± 3.0 %, 68 ± 2.7 %, and 73 ± 5.9 % in crusts, paved sediments, sediments, and dunes, respectively), followed by the FeD percentage from FeT (FeD / FeT) (31 ± 2.3 %, 29 ± 3.0 %, 30 ± 3.0 %, 26 ± 5.8 %), and the FeA percentage from FeT (FeA / FeT) (1.9 ± 0.55 %, 1.7 ± 0.56 %, 1.4 ± 0.55 %, and

Proof only

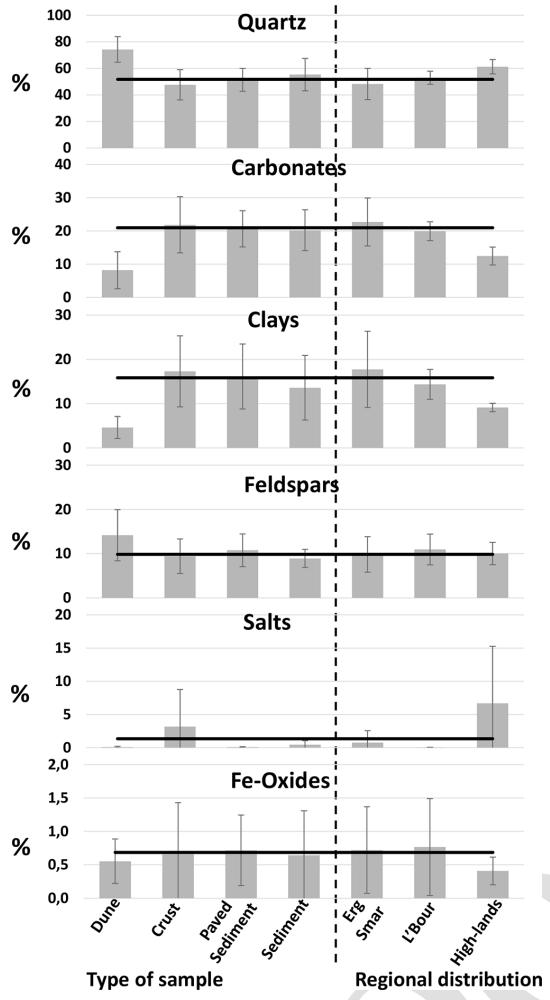

Figure 6. Mean mineral group content of dune, crust, paved sediment and sediment samples, and also at Erg Smar and L'Bour and in the highlands. Solid lines mark the mean content of all the samples (excluding dune samples). The dashed line divides between type and location of the samples.

1.0 ± 0.54 %). These results show that FeT is very similar between crusts, paved sediments, and sediments, while FeT in dunes is depleted by almost 50 %. Compared to the samples by Shi et al. (2011) from north-western Africa, the samples of this study are depleted in total iron (4.7 % FeT from Shi et al. (2011)), quite similar in FeS (67 % from Shi et al. (2011)), similar in FeD (33 % from Shi et al. (2011)), and much higher in FeA (0.43 % from Shi et al. (2011)).

The mean FeT content in the basin is similar in Erg Smar (3.6 ± 0.27 %) and L'Bour (3.2 ± 0.66 %) compared to highlands (3.0 ± 0.24 %). The ratio FeA / FeT was slightly higher at Erg Smar (1.9 ± 0.53 %) but similar at L'Bour and in the highlands (1.3 ± 0.44 % and 1.5 ± 0.47 %, respectively). This is probably due to the preferential accumulation of exchangeable and nano-Fe oxides (FeA) in the lowlands, where flooding results in red-water ponds and red surfaces after drying. Subsequently, highly concentrated ionic Fe is trapped in the last stages of ponding, and nano-Fe oxides may precipitate during drying. Once the ponded is dried, the crusts of the lowlands tend to have a reddish patina (see Sect. 3.4). However, a slightly higher mean FeD / FeT of 33 ± 2.4 % is obtained in the highlands compared to 31 ± 2.7 % and 29 ± 2.4 % at L'Bour and Erg Smar, respectively. The FeS / FeT mean content is slightly lower in the highlands (65 ± 2.5 %) compared to Erg Smar and L'Bour (69 ± 2.6 % and 68 ± 2.6 %, respectively).

FeD levels were apportioned between hematite and goethite using XRD proportions. These results show that in crusts, 0.79 ± 0.66 % of hematite and 0.55 ± 0.67 % of goethite are present, in paved sediments 0.83 ± 0.51 % and 0.64 ± 0.54 %, in sediments 0.73 ± 0.58 % and 0.69 ± 0.59 %, and in dunes 0.20 ± 0.17 % and 0.68 ± 0.24 %.

The proportions of FeD + FeA are higher in crusts, probably due to preferential transport of non-FeS to the lowlands and the trapping of Fe ions (FeA) by clay adsorption during ponding and the formation of nano-sized ferrihydrite ($Fe_{4–5}(OH,O)_{12}$. This readily exchangeable Fe has very low impact on radiative forcing but a high impact on Fe fertilisation of oceans during dust events (Gobler et al., 2001), as ionic Fe adsorbed by clays and nano-Fe oxides are easily released in water solutions. The correlation of FeS, FeD, and FeA with FeT is linear, with coefficients of determination (R^2) reaching 0.96, 0.89, and 0.67 for FeS, FeD, and FeA respectively (Fig. S5). Thus, when increasing total Fe content, all modes of occurrence of Fe increase, but the increase is preferentially driven by FeS, while it seems that the basin FeA segregation causes a lower correlation with FeT.

3.4 Conceptual model for particle size and mineralogy fractionation in crusts and paved sediments

According to Bullard et al. (2011), and as previously discussed in this study, heavy rainfall results in the selective deposition of coarser particles from runoff and floodwaters in higher elevations. Conversely, smaller particles enriched in clays, colloidal Fe oxides (which give the water a reddish hue), and dissolved salts tend to be transported to lower elevations. Figure 7 summarises a conceptual model that outlines the formation of crusts and paved sediment in the study area, with a focus on particle size and mineralogical fractionation.

In the lowlands, floodwaters carrying fine sediments flood extensive flat areas, such as Erg Smar or Lake Iriki. Prospero et al. (2002), Bullard et al. (2011), and Ginoux et al. (2012), among others, have shown that dust emissions originate from relatively small and localised areas where sediments are supplied by floodwaters and that the occurrence of dust emissions from these areas may be partly due to the occurrence or absence of flooding. During ponding in the lowlands, coarser particles deposit first and form a high sand-rich bottom layer

Proofonly

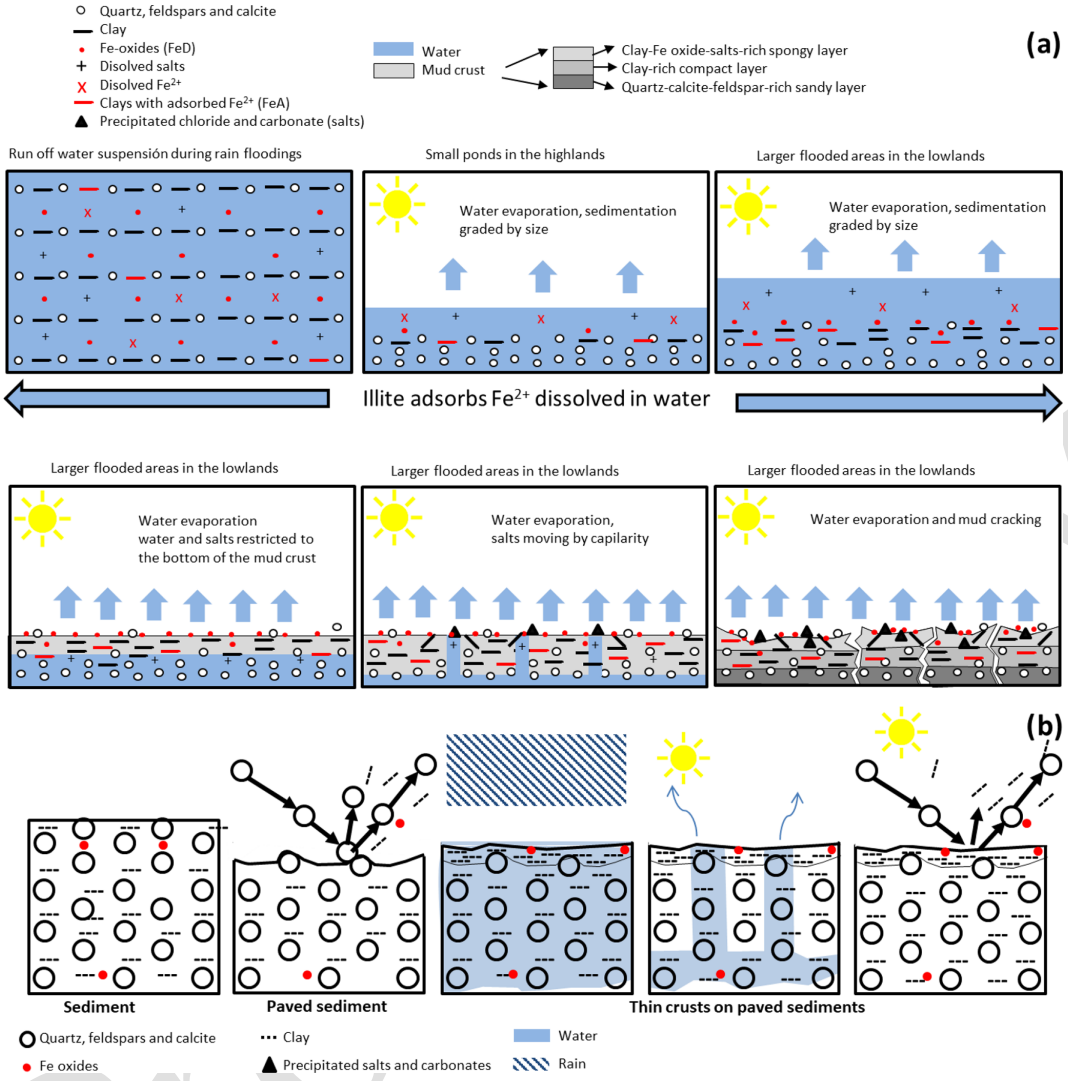

Figure 7. Schematic model of sedimentation and deposition processes in the study site from the highlands to lowlands for **(a)** crusts and for **(b)** paved sediments.

of the crust (as described in Sect. 3.2) (Figs. 7a and 8a). Subsequently, the clay fraction deposits on top of the bottom layer until total dryness (Figs. 7a and 8a), forming a second clay-rich fraction layer in the crust. However, the particle size in crust surfaces is heterogeneous (Figs. S6 and S7), which can result in erodible dust-emitting sediment (heterogeneity enhances sandblasting). The finer and more easily exchangeable FeA fraction remains in suspension until the last drying stages on the most superficial layer of the crust, during drying out of the remaining ponds (as described in Sect. 3.3) (Figs. 7a and 8a). During this ponding, dissolved Fe ions interact with clays in such a way that they can be adsorbed on clay surfaces according to the ionic composition of the waters (as described in Sect. 3.3) (Echeverría et al., 1998). This typical ion adsorption by clays is higher for montmorillonite than for other clays but the content of montmorillonite is low compared to illite. In this study a high correlation is obtained for FeA and illite contents (Fig. S8). Furthermore, crusts contain a higher proportion of hematite(oxide) / goethite(hydroxide) in the FeD, due to the weathering with water during transport and ponding and precipitation of nano-Fe oxides during drying.

After the pond drying, the continuous heating of the clay rich surface layer causes the hardening of the crust and mud-cracking, giving a "ceramic-like" compactness to the thick crusts in the lowlands, usually with a reddish colour induced by the Fe oxides (Fig. S6a). Complete drying causes mud cracks due to loss of volume, breaking the crust into polygonal pieces, whose thickness and area depend on the amount of clay deposited. Furthermore, these concave mud-crust pieces resulting from the cracking usually have a grey-colour patch in the middle due to the superficial precipita-

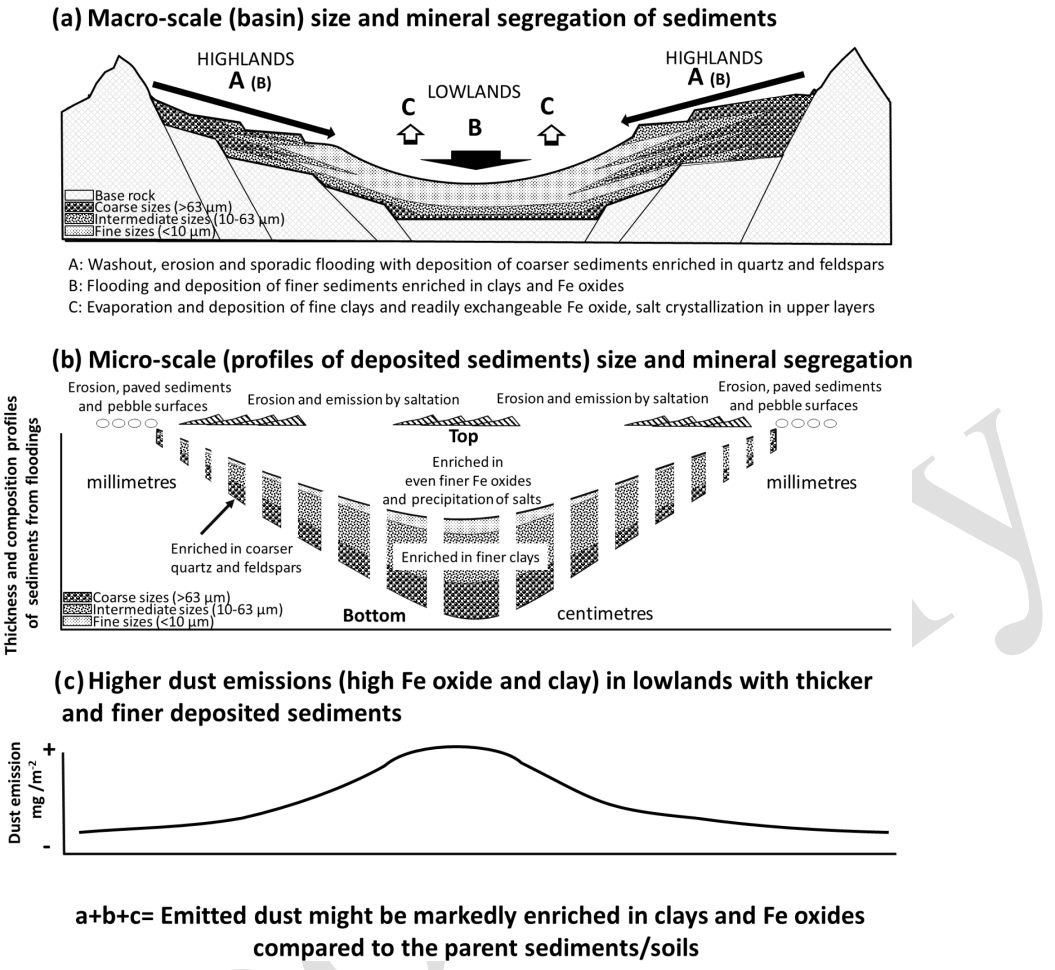

Figure 8. Dust emission conceptual model integrating particle-size distributions and mineralogy of dust hotspots sediments. Panel **(a)** refers to the conceptual thickness and particle-size distributions along the basin, **(b)** to the particle-size distribution and segregation of mineralogy, and **(c)** to the dust emission quantity expected depending on the place in the basin.

tion of salts, which together with carbonates accumulate by capillarity (see Sect. 3.1.2) (Fig. S6b). This capillary ascension and precipitation of salts (the latter being an expansive process) causes sponging and breaking of the surface layers. Thus, a third (top) layer is formed in the crusts of the lowlands, which is very easily eroded by wind because of the spongy structure and enriched in clay and readily exchangeable Fe. In some cases, in Erg Smar, an additional breaking and sponging of the third (upper layer), due to expansive clays, was observed. Both the ceramic-like compactness and the cementing of salts give the fine-clay rich crusts in the lowlands a compact pattern with coarser MDPSD compared with the highlands, where ponding is limited and very thin crusts occur. This could explain why the crusts from the lowlands have finer FDPSDs and coarser MDPSDs compared to the highlands (see Sect. 3.1.1). Also, wind erosion of the few top millimetres of these crusts may result in dust with higher contents of clay, Fe oxide, and salts compared to a 15 cm sediment profile.

In the highlands, washout erosion occurs during rainfall, leading to the formation of very thin crusts in reduced areas. This results in sources of dust made of very thin crusts and fields of stony surfaces with lower emission rates compared to the lowlands (Bullard et al., 2011). As illustrated in Fig. S7, the surfaces of paved sediments and their thin crusts might resemble crusts profiles but with the top section depleted on clay minerals due to preferential erosion over time and with a very thin layer (a few micrometres) of clay minerals from the previous intact formed crust after flooding or running water. The top paved sediments are more compact and finer and have a homogeneous distribution of the particles compared to crusts, which makes them less erodible and less likely to emit dust compared to crusts (which have heterogeneous particle size; see Sect. 3.2).

4 Conclusions

This study analysed the particle size and mineralogy of dust-emitting sediments in the region of the Drâa basin in northern Africa, at the north-western fringe of the Sahara. The study aimed to compare these patterns for different types of dust-emitting sediments and their variations across the basin. The results are consistent with the conceptual models of dust emission sources in desert areas of Prospero et al. (2002) and Bullard et al. (2011), which predict higher dust emissions in the lowlands than in the highlands. The study shows a clear size and mineralogical fractionation between paleo-sediments and lowland dust-emitting sediments, indicating that collecting samples of parent paleo-sediments for particle size and mineralogy may not fully represent the dust emission hotspots.

Both PSDs and mineralogy are segregated by transport and deposition of sediments during runoff of water across the basin and by the precipitation of salts, which causes a sedimentary fractionation. Coarser particles such as quartz, feldspars, and carbonates (detrital) deposit first due to friction and gravity and are enriched in the highlands. In contrast, waters reaching the lowlands are enriched in fine particles (clays), carbonate, salt, and Fe ions from partial dissolution of minerals of the source lands. When these waters are ponded in lowlands, coarser minerals deposit first, followed by a second layer enriched in clays minerals. Evaporation of the last ponded water layer causes the deposition of the finest particles and clays enriched in readily exchangeable ions of Fe. Once dried, the heating of the surfaces by insolation causes evaporation of interstitial solutions moving towards the surface by capillarity, leading to the precipitation of salts and secondary carbonates in the upper layer. This expansive process sponges the surface of the crust, in some cases accelerated by the occurrence of expansive clays, which might favour dust emission from a top micro-layer rich in clay, Fe, and salts. Therefore, dust emission is not only higher but also has a different mineral composition in the lowlands than in the highlands that is also controlled by the type of sediment.

The results of this study show that modelling mineral-speciated dust emission requires understanding of the mineralogical and particle-size fractionation of accumulated sediments across inland enclosed basins. Large areas may act as sediment suppliers, while reduced areas may act as dust emitters with differences in sediment composition. Models that represent mineral-speciated dust emission and transport should be developed to properly account for these factors.

The results have also shown that global atlases overestimate the clay mineral content and underestimate that of quartz, feldspars, and Fe oxides. Quartz and feldspars are overestimated and clay minerals underestimated in the silt-size fractions. Kaolinite and chlorite are not differentiated, while this study finds major differences. The classical procedure loses salts during fractionation, and Fe oxides are detected mainly by colour without precision. This study detects dolomite, palygorskite, and smectite and provides more precision for Fe oxides, with the mode of occurrence of Fe in different types of samples and locations. However, the study was unable to obtain a sample below 10 µm without losing salts in the process.

Dust models need global observationally constrained high-resolution mineral maps, which will soon become available based on high-quality spaceborne spectroscopy measurements performed from the International Space Station (Fig. 1c, Green et al., 2020). A key challenge of mineral mapping based on spectroscopy for dust emission modelling is to constrain not only the presence (Fig. 1c) but also the abundance of the different surface minerals. The data gathered and analysed in this study will be used to evaluate these spaceborne retrievals in forthcoming studies.

The large dam built in the Drâa River has caused the drying of this part of the basin, a reduction of vegetation, and probably increased dust emissions. The region exemplifies how anthropogenic activities can promote wind erosion and represents a unique location for research on the topic. Future studies may indeed explore many other aspects related to sedimentology, mineralogy, wind erosion, dust emission, and anthropogenic impacts, including the study of the introduction of native plants and green belts to reduce wind erosion, as has already been done in other regions (Al-Dousari et al., 2020).

Code availability. The code used in this paper is provided by Clark (2023, https://github.com/PSI-edu/spectroscopy-tetracorder).

Data availability. Data used in this paper are given in the main paper itself and in the Supplement. If needed, data are also available upon request by emailing the authors.

Supplement. The supplement related to this article is available online at: https://doi.org/10.5194/acp-23-1-2023-supplement.

Author contributions. CPGP proposed and designed the field campaign with contributions of AA, KK, MK, and XQ. The campaign was implemented by CPGP, AA, CGF, AGR, KK, MK, AP, XQ, CR, and JYD. The samples were collected by CPGP, AA, AGR, MK, and XQ and analysed by CB, PC, AGR, CR, NM, and ZS. Spectroscopy was analysed by RNC. AGR performed the visualisation and writing of the original draft manuscript, and CPGP and XQ supervised the work. CPGP and XQ re-edited the manuscript, and all authors contributed to the data discussion, review, and manuscript finalisation.

Competing interests. At least one of the (co-)authors is a member of the editorial board of *Atmospheric Chemistry and Physics*.

Proof only

The peer-review process was guided by an independent editor, and the authors also have no other competing interests to declare.

Disclaimer. Publisher's note: Copernicus Publications remains neutral with regard to jurisdictional claims made in the text, published maps, institutional affiliations, or any other geographical representation in this paper. While Copernicus Publications makes every effort to include appropriate place names, the final responsibility lies with the authors.

Acknowledgements. The field campaign and its associated research, including this work, was primarily funded by the European Research Council under the Horizon 2020 Research and Innovation programme through the ERC Consolidator Grant FRAGMENT (grant agreement no. 773051) and the AXA Research Fund through the AXA Chair on Sand and Dust Storms at BSC. Cristina González-Florez was supported by a PhD fellowship from the Agència de Gestió d'Ajuts Universitaris i de Recerca (AGAUR) (grant no. 2020_FI B 00678). Konrad Kandler was funded by the Deutsche Forschungsgemeinschaft (DFG, German Research Foundation; grant nos. 264907654 and 416816480). Martina Klose has received funding through the Helmholtz Association's Initiative and Networking Fund (grant agreement no. VH-NG-1533).

The authors acknowledge the EMIT project, which is supported by the NASA Earth Venture Instrument program, under the Earth Science Division of the Science Mission Directorate. The authors thank Santiago Beguería from the National Scientific Council of Spain for facilitating a field site in Zaragoza, Spain, to test the field instrumentation and procedures prior to the campaign in Morocco. The authors thank Paul Ginoux for providing high-resolution global dust-source maps, which were very helpful for the identification of the FRAGMENT experimental sites. The authors thank Kamal Taj Eddine from Cady Ayyad University, Marrakesh, Morocco, for his invaluable support and suggestions for the preparation of the field campaign. The authors thank Bethany L. Ehlmann and Rebecca Greenberger for their help collecting samples and doing infrared in situ spectroscopy and discussion analysis and Abigail M. Keebler for discussion analysis. The authors thank Houssine Dakhamat and the crew of Hotel Chez le Pacha in M'hamid El Ghizlane for their support during the campaign.

Financial support. This research has been supported by the European Research Council, H2020 European Research Council (grant no. 773051); the AXA Research Fund (Chair on Sand and Dust Storms at BSC); the Agència de Gestió d'Ajuts Universitaris i de Recerca (grant no. 2020_FI B 00678); the Deutsche Forschungsgemeinschaft (grant no. 264907654); and the Helmholtz Association (grant no. VH-NG-1533).

We acknowledge support of the publication fee by the CSIC Open Access Publication Support Initiative through its Unit of Information Resources for Research (URICI).

Review statement. This paper was edited by Yves Balkanski and reviewed by Ali Al-Dousari and one anonymous referee.

References

Al-Dousari, A., Ibrahim, M. I., Al-Dousari, N., Ahmed, M., and Al-Awadhi, S.: Pollen in aeolian dust with relation to allergy and asthma in Kuwait, Aerobiologia, 34, 325–336, 2018.

Al-Dousari, A., Alsaleh, A., Ahmed, M., Misak, R., Al-Dousari, N., Al-Shatti, F., Elrawi, M., and William, T.: Off-road vehicle tracks and grazing points in relation to soil compaction and land degradation, Earth Syst. Environ., 3, 471–482, 2019.

Al-Dousari, A., Ramadan, A., Al-Qattan, A., Al-Ateeqi, S., Dashti, H., Ahmed, M., Al-Dousari, N., Al-Hashash, N., and Othman, A.: Cost and effect of native vegetationchange on aeolian sand, dust, microclimate and sustainable energy in Kuwait, J. Taibah Univ. Sci., 14, 628–639, 2020.

Al-Ghadban, A. N., Saeed, T., Al-Dousari, A., Al-Shemmari, H., and Al-Mutairi, M.: Preliminary assesment of the impact of draining of iraqi marshes on kuwait's northern marine environment. part I. Physical manipulation, Water Sci. Technol., 40, 75–87, 1999.

Alshemmari, H., Al-Dousari, A., Talebi, L., and Al-Ghadban, A. N.: Mineralogical characteristics of surface sediment in Sulaibikhat Bay, Kuwait, Kuwait J. Sci., 40, 159–176, 2013.

Baddock, M. C., Ginoux, P., Bullard, J. E., and Gill, T. E.: Do MODIS-defined dust sources have a geomorphological signature?, Geophys. Res. Lett., 43, 2606–2613, https://doi.org/10.1002/2015GL067327, 2016.

Bauer, S. E., Balkanski, Y., Schulz, M., Hauglustaine, D. A., and Dentener, F.: Global modeling of heterogeneous chemistry on mineral aerosol surfaces: Influence on tropospheric ozone chemistry and comparison to observations, J. Geophys. Res.-Atmos., 109, D02304, https://doi.org/10.1029/2003JD003868, 2004.

Berger, E., Bossenbroek, L., Beermann, A. J., Schäfer, R. B., Znari, M., Riethmüller, S., Sidhu, N., Kaczmarek, N., Benaissa, H., Ghamizi, M., Plicht, S., Salem, S. B., El Qorchi, F., Naimi, M., Leese, F., and Frör, O.: Social-ecological interactions in the Draa River Basin, southern Morocco: Towards nature conservation and human well-being using the IPBES framework, Sci. Total Environ., 769, 144492, https://doi.org/10.1016/j.scitotenv.2020.144492, 2021.

Boose, Y., Sierau, B., García, M. I., Rodríguez, S., Alastuey, A., Linke, C., Schnaiter, M., Kupiszewski, P., Kanji, Z. A., and Lohmann, U.: Ice nucleating particles in the Saharan Air Layer, Atmos. Chem. Phys., 16, 9067–9087, https://doi.org/10.5194/acp-16-9067-2016, 2016.

Boyd, P. W., Jickells, T., Law, C. S., Blain, S., Boyle, E.,A., Buesseler, K. O., Coale, K. H., Cullen, J. J., De Baar, H. J. W., Follows, M., Harvey, M., Lancelot, C., Levasseur, M., Owens, N. P. J., Pollard, R., Rivkin, R. B., Sarmiento, J., Schoemann, V., Smetacek, V., Takeda, S., Tsuda, A., Turner, S., and Watson, A. J.: Mesoscale Iron Enrichment Experiments 1993–2005: Synthesis and Future Directions, Science, 315, 612–617, 2007.

Bullard, J. E., Harrison, S. P., Baddock, M. C., Drake, N., Gill, T. E., McTainsh, G., and Sun, Y.: Preferential dust source: A geomorphological classification designed for use in global dust-cycle models, J. Geophys. Res., 116, F04034, https://doi.org/10.1029/2011JF002061, 2011.

Caquineau, S., Gaudichet, A., Gomes, L., Magonthier, M. C., and Chatenet, B.: Saharan dust: Clay ratio as a relevant tracer to as-

Proof only

sess the origin of soil derived aerosols, Geophys. Res. Lett., 25, 983–986, 1998.

Cattle, S. R., McTainsh, G. H., and Wagner, S.: Aeolian dust contributions to soil of the Namoi Valley, northern NSW, Australia, Catena, 47, 245–264, 2002.

Chung, F. H.: Quantitative Interpretation of X-Ray Diffraction Patterns of Mixtures. I. Matrix-Flushing Method for Quantitative Multicomponent Analysis, J. Appl. Crystallogr., 7, 519–525, 1974.

Claquin, T., Schulz, M., and Balkanski, Y. J.: Modeling the mineralogy of atmospheric dust sources, J. Geophys. Res., 104, 22243–22256, 1999.

Clark, R. N., Swayze, G. A., Livo, K. E., Kokaly, R. F., Sutley, S. J., Dalton, J. B., McDougal, R. R., and Gent, C. A.: Imaging spectroscopy: Earth and planetary remote sensing with the USGS Tetracorder and expert systems, J. Geophys. Res., 108, 5131, https://doi.org/10.1029/2002JE001847, 2003.

Clark, R. N.: Tetracorder, GitHub [code], https://github.com/PSI-edu/spectroscopy-tetracorder (last access: 6 June 2023), 2023.

Chatenet, B., Marticorena, B., Gomes, L., and Bergametti, G.: Assessing the microped size distributions of desert soils erodible by wind, Sedimentology, 43, 901–911, 1996.

De Longueville, F., Hountondji, Y. C., Henry, S., and Ozer, P.: What do we know about effects of desert dust on air quality and human health in West Africa compared to other regions?, Sci. Total Environ., 409, 1–8, 2010.

Di Biagio, C., Formenti, P., Balkanski, Y., Caponi, L., Cazaunau, M., Pangui, E., Journet, E., Nowak, S., Andreae, M. O., Kandler, K., Saeed, T., Piketh, S., Seibert, D., Williams, E., and Doussin, J.-F.: Complex refractive indices and single-scattering albedo of global dust aerosols in the shortwave spectrum and relationship to size and iron content, Atmos. Chem. Phys., 19, 15503–15531, https://doi.org/10.5194/acp-19-15503-2019, 2019.

Doronzo, D. M., Al-Dousari, A., and Folch, A., Dagsson-Waldhauserova: Preface to the Dust Topical Collection, Arab. J. Geosci., 9, 468, https://doi.org/10.1007/s12517-016-2504-9, 2016.

Echeverría, J. C., Morera, M. T., Mazkiarán, C., and Garrido, J. J.: Competitive sorption of heavy metal by soils. Isotherms and fractional factorial experiments, Environ. Pollut., 101, 275–284, https://doi.org/10.1016/S0269-7491(98)00038-4, 1998.

Engelbrecht, J. P., Moosmüller, H., Pincock, S., Jayanty, R. K. M., Lersch, T., and Casuccio, G.: Technical note: Mineralogical, chemical, morphological, and optical interrelationships of mineral dust re-suspensions, Atmos. Chem. Phys., 16, 10809–10830, https://doi.org/10.5194/acp-16-10809-2016, 2016.

Etzler, F. M. and Deanne, R.: Particle Size Analysis: A comparison of Various Methods, Part II, Cyst. Charact., 14, 278–282, 1997.

FAO-UNESCO: Food & Agriculture Organization-United Nations Educational Scientific, and Cultural Organization: Guidelines for soil description, 3rd edition, Journal FAO & ISRIC, Rome, ISBN 92-5-105521-1, 1990.

Formenti, P., Rajot, L., Desboeufs, K., Caquineau, S., Chevaillier, S., Nava, S., Gaudichet, A., Journet, E., Triquet, S., Alfaro, S., Chiari, M., Haywood, J., Coe, H., and Highwood, E.: Regional variability of the composition of mineral dust from western Africa: Results from the AMMA SOP0/DABEX and DODO field campaigns, J. Geophys. Res., 113, D00C13, https://doi.org/10.1029/2008JD009903, 2008.

Gillette, D. A.: A qualitative geophysical explanation for hot spot dust emitting source regions, Contrib. Atmos. Phys., 72, 67–77, 1999.

Ginoux, P., Chin, M., Tegen, I., Prospero, J. M., Holben, B., Dubovik, O., and Lin, S.-J.: Sources and distributions of dust aerosols simulated with the GOCART model, J. Geophys. Res.-Atmos., 106, 20255–20273, 2001.

Ginoux, P., Prospero, J. M., Gill, T. E., Hsu, N. C., and Zhao, M.: Global-scale attribution of anthropogenic and natural dust sources and their emission rates based on MODIS Deep Blue aerosol products, Rev. Geophys., 50, RG3005, https://doi.org/10.1029/2012RG000388, 2012.

Gobler, C. J. and Sañudo-Wilhelmy, S. A.: Effects of organic nitrogen, inorganic nutrients, and iron additions on the growth of phytoplankton and bacteria during a brown tide bloom, Mar. Ecol. Prog. Ser., 209, 19–34, 2001.

Gonçalves Ageitos, M., Obiso, V., Miller, R. L., Jorba, O., Klose, M., Dawson, M., Balkanski, Y., Perlwitz, J., Basart, S., Di Tomaso, E., Escribano, J., Macchia, F., Montané, G., Mahowald, N. M., Green, R. O., Thompson, D. R., and Pérez García-Pando, C.: Modeling dust mineralogical composition: sensitivity to soil mineralogy atlases and their expected climate impacts, Atmos. Chem. Phys., 23, 8623–8657, https://doi.org/10.5194/acp-23-8623-2023, 2023.

González-Flórez, C., Klose, M., Alastuey, A., Dupont, S., Escribano, J., Etyemezian, V., Gonzalez-Romero, A., Huang, Y., Kandler, K., Nikolich, G., Panta, A., Querol, X., Reche, C., Yus-Díez, J., and Pérez García-Pando, C.: Insights into the size-resolved dust emission from field measurements in the Moroccan Sahara, Atmos. Chem. Phys., 23, 7177–7212, https://doi.org/10.5194/acp-23-7177-2023, 2023.

Goudie, A. S. and Middleton, N. J.: Desert dust in the global system, Springer, Heidelberg, 288 pp., ISBN 978-3-540-32355-6, 2006.

Green, R. O., Mahowald, N., Ung, C., Thompson, D. R., Bator, L., Bennet, M., and Zan, J.: The earth surface mineral dust source investigation: an earth science imaging spectroscopy mission, in: IEEE Aerospace Conference Proceedings, IEEE Computer Society, Big Sky, MT, USA, 7–14 March 2020, https://doi.org/10.1109/AERO47225.2020.9172731, 2020.

Grider, A., Ponette-González, A., and Heindel, R.: Calcium and ammonium now control the pH of wet and bulk deposition in Ohio, US, Atmos. Environ., 310, 119986, https://doi.org/10.1016/j.atmosenv.2023.119986, 2023.

Harrison, A. D., Lever, K., Sanchez-Marroquin, A., Holden, M. A., Whale, T. F., Tarn, M. D., McQuaid, J. B., and Murray, B. J.: The ice-nucleating ability of quartz immersed in water and its atmospheric importance compared to K-feldspar, Atmos. Chem. Phys., 19, 11343–11361, https://doi.org/10.5194/acp-19-11343-2019, 2019.

Horváth, B., Opara-Nadi, O., and Beese, F.: A simple method for measuring the carbonate content of soils, Soil Sci. Soc. Am. J., 69, 593–604, 2005.

Ito, A. and Wagai, R.: Global distribution of clay-size minerals on land surface for biogeochemical and climatological studies, Sci. Data, 4, 170103, https://doi.org/10.1038/sdata.2017.103, 2017.

Proof only

Journet, E., Balkanski, Y., and Harrison, S. P.: A new data set of soil mineralogy for dust-cycle modeling, Atmos. Chem. Phys., 14, 3801–3816, https://doi.org/10.5194/acp-14-3801-2014, 2014.

Karanasiou, A., Moreno, N., Moreno, T., Viana, M., de Leeuw, F., and Querol, X.: Health effects from Sahara dust episodes in Europe: Literature review and research gaps, Environ. Int., 47, 107–14, 2012.

Klose, M., Jorba, O., Gonçalves Ageitos, M., Escribano, J., Dawson, M. L., Obiso, V., Di Tomaso, E., Basart, S., Montané Pinto, G., Macchia, F., Ginoux, P., Guerschman, J., Prigent, C., Huang, Y., Kok, J. F., Miller, R. L., and Pérez García-Pando, C.: Mineral dust cycle in the Multiscale Online Nonhydrostatic AtmospheRe CHemistry model (MONARCH) Version 2.0, Geosci. Model Dev., 14, 6403–6444, https://doi.org/10.5194/gmd-14-6403-2021, 2021.

Kok, J. F., Adebiyi, A. A., Albani, S., Balkanski, Y., Checa-Garcia, R., Chin, M., Colarco, P. R., Hamilton, D. S., Huang, Y., Ito, A., Klose, M., Li, L., Mahowald, N. M., Miller, R. L., Obiso, V., Pérez García-Pando, C., Rocha-Lima, A., and Wan, J. S.: Contribution of the world's main dust source regions to the global cycle of desert dust, Atmos. Chem. Phys., 21, 8169–8193, https://doi.org/10.5194/acp-21-8169-2021, 2021.

Li, L., Mahowald, N. M., Miller, R. L., Pérez García-Pando, C., Klose, M., Hamilton, D. S., Gonçalves Ageitos, M., Ginoux, P., Balkanski, Y., Green, R. O., Kalashnikova, O., Kok, J. F., Obiso, V., Paynter, D., and Thompson, D. R.: Quantifying the range of the dust direct radiative effect due to source mineralogy uncertainty, Atmos. Chem. Phys., 21, 3973–4005, https://doi.org/10.5194/acp-21-3973-2021, 2021.

Middleton, N. J.: Desert dust hazards: A global review, Aeolian Res., 24, 53–63, 2017.

Monteiro, A., Basart, S., Kazadzia, S., Votsis, A., Gkikas, A., Vandenbussche, S., Tobias, A., Gama, C., Pérez García-Pando, C., Terradellas, E., Notas, G., Middleton, N., Kushta, J., Amiridis, V., Lagouvardos, K., Kosmopoulos, P., Kotroni, V., Kanakidou, M., Mihalopoulos, N., Kalivitis, N., Dagsson-Waldhauserová, P., El-Askary, H., Sievers, K., Giannaros, T., Mona, L., Hirtl, M., Skomorowski, P., Virtanen, T. H., Christoudias, T., Di Mauro, B., Tripetta, S., Kutuzov, S., Meinander, O., and Nickovic, S.: Multi-sectorial impact assessment of an extreme African dust episode in the Eastern Mediterranean in March 2018, Sci. Total Environ., 843, 156861, https://doi.org/10.1016/j.scitotenv.2022.156861, 2022.

Nickovic, S., Vukovic, A., Vujadinovic, M., Djurdjevic, V., and Pejanovic, G.: Technical Note: High-resolution mineralogical database of dust-productive soils for atmospheric dust modeling, Atmos. Chem. Phys., 12, 845–855, https://doi.org/10.5194/acp-12-845-2012, 2012.

Panta, A., Kandler, K., Alastuey, A., González-Flórez, C., González-Romero, A., Klose, M., Querol, X., Reche, C., Yus-Díez, J., and Pérez García-Pando, C.: Insights into the single-particle composition, size, mixing state, and aspect ratio of freshly emitted mineral dust from field measurements in the Moroccan Sahara using electron microscopy, Atmos. Chem. Phys., 23, 3861–3885, https://doi.org/10.5194/acp-23-3861-2023, 2023.

Paulot, F., Ginoux, P., Cooke, W. F., Donner, L. J., Fan, S., Lin, M.-Y., Mao, J., Naik, V., and Horowitz, L. W.: Sensitivity of nitrate aerosols to ammonia emissions and to nitrate chemistry: implications for present and future nitrate optical depth, Atmos. Chem. Phys., 16, 1459–1477, https://doi.org/10.5194/acp-16-1459-2016, 2016.

Pérez, C., Haustein, K., Janjic, Z., Jorba, O., Huneeus, N., Baldasano, J. M., Black, T., Basart, S., Nickovic, S., Miller, R. L., Perlwitz, J. P., Schulz, M., and Thomson, M.: Atmospheric dust modeling from meso to global scales with the online NMMB/BSC-Dust model – Part 1: Model description, annual simulations and evaluation, Atmos. Chem. Phys., 11, 13001–13027, https://doi.org/10.5194/acp-11-13001-2011, 2011.

Pérez García-Pando, C., Stanton, M. C., Diggle, P. J., Trzaska, S., Miller, R. L., Perlwitz, J. P., Baldasano, J. M., Cuevas, E., Ceccato, P., Yaka, P., and Thomson, M. C.: Soil dust aerosols and wind as predictors of seasonal meningitis incidence in Niger, Environ. Health Persp., 122, 7679–686, 2014.

Perlwitz, J. P., Pérez García-Pando, C., and Miller, R. L.: Predicting the mineral composition of dust aerosols – Part 1: Representing key processes, Atmos. Chem. Phys., 15, 11593–11627, https://doi.org/10.5194/acp-15-11593-2015, 2015.

Prospero, J. M., Ginoux, P., Torres, O., Nicholson, S. E., and Gill, T. E.: Environmental characterization of global sources of atmospheric soil dust identified with the Nimbus 7 Total Ozone Mapping Spectrometer (TOMS) absorbing aerosol product, Rev. Geophys., 40, 1002, https://doi.org/10.1029/2000RG000095, 2002.

Pye, K. and Tsoar, H.: The mechanics and geological implications of dust transport and deposition in deserts with particular reference to loess formation and dune sand diagenesis in the northern Negev, Israel. Geol. Soc. Of London Publ., 139–156, https://doi.org/10.1144/GSL.SP.1987.035.01.10, 2015.

Querol, X.: The Occurrence and Distribution of Trace Elements in the Teruel Mining District Coals and their Behaviour during Coal Combustion, European Coal and Steel Community Project 7220/ED/014, 1993.

Querol, X., Whateley, M. K. G., Fernandez-Turiel, J. L., and Tuncalim, E.: Geological controls on the mineralogy and geochemistry of the Beypazari lignite, Central Anatolia, Turkey, Int. J. Coal. Geol., 33, 255–271, 1997.

Querol, X., Tobías, A., Pérez, N., Karanasiou, A., Amato, F., Stafoggia, M., Pérez García-Pando, C., Ginoux, P., Forastiere, F., Gumy, S., Mudu, P., and Alastuey, A.: Monitoring the impact of desert dust outbreaks for air quality for health studies, Environ. Int., 130, 104867, https://doi.org/10.1016/j.envint.2019.05.061, 2019.

Reynolds, R. L., Cattle, S. R., Moskowitz, B. M., Goldstein, H. L., Yauk, K., Flagg, C. B., Berquó, T. S., Kokaly, R. F., Morman, S., and Breit, G. N.: Iron oxide minerals in dust of the Red Dawn event in eastern Australia, September 2009, Aeolian Res., 15, 1–13, 2014.

Scanza, R. A., Mahowald, N., Ghan, S., Zender, C. S., Kok, J. F., Liu, X., Zhang, Y., and Albani, S.: Modeling dust as component minerals in the Community Atmosphere Model: development of framework and impact on radiative forcing, Atmos. Chem. Phys., 15, 537–561, https://doi.org/10.5194/acp-15-537-2015, 2015.

Scheuvens, D., Schütz, L., Kandler, K., Ebert, M., and Weinbruch, S.: Bulk composition of northern African dust and its source sediments – A compilation, Earth-Sci. Rev., 116, 170–194, 2013.

Shao, Y., Ishizuka, M., Mikami, M., and Leys, J. F.: Parameterization of size-resolved dust emission and valida-

Proof Only

tion with measurements, J. Geophys. Res., 116, D08203, https://doi.org/10.1029/2010JD014527, 2011.

Shen, Z., Caquineau, S., Cao, J., Zhang, X., Hana, Y., Gaudichet, A., and Gomes, L.: Mineralogical characteristics of soil dust from source regions in northern China, Particuology, 7, 507–512, 2009.

Shi, Z., Krom, M. D., Bonneville, S., Baker, A. R., Bristow, C., Drake, N., Mann, G., Carslaw, K., McQuaid, J. B., Jickells, T., and Benning, L. G.: Influence of chemical weathering and aging of iron oxides on the potential iron solubility of Saharan dust during simulated atmospheric processing, Global Biogeochem. Cy., 25, GB2010, https://doi.org/10.1029/2010GB003837, 2011.

Shi, Z. B., Krom, M. D., and Bonneville, S.: Formation of Iron Nanoparticles and Increase in Iron Reactivity in Mineral Dust during Simulated Cloud Processing, Environ. Sci. Technol., 43, 6592–6596, 2009.

Shi, Z. B., Krom, M. D., Jickells, T. D., Bonneville, S., Carslaw, K. S., Mihalopoulos, N., Baker, A. R., and Benning, L. G.: Impacts on iron solubility in the mineral dust by processes in the source region and the atmosphere: A review, Aeolian Res., 5, 21–42, https://doi.org/10.1016/j.aeolia.2012.03.001, 2012.

Sokolik, I. N. and Toon, O. B.: Incorporation of mineralogical composition into models of the radiative properties of mineral aerosol from UV to IR wavelengths, J. Geophys. Res., 104, 9423–9444, 1999.

Sperazza, M., Moore, J. N., and Hendrix, M.: High-Resolution particle size analysis of naturally occurring very fine-grained sediment through laser diffractometry, J. Sediment. Res., 74, 736–743, 2004.

Stout, J. E. and Lee, J. A.: Indirect evidence of wind erosion trends on the Southern High Plains of North America, J. Arid Environ., 55, 43–61, 2003.

Subramaniam, N., Al-Sudairawi, M., Al-Dousari, A., and Al-Dousari, N.: Probabilty distribution and extreme value analysis of total suspended particulate matter in Kuwait, Arab. J. Geosci., 8, 11329–11344, https://doi.org/10.1007/s12517-015-2008-z, 2015.

Sullivan, R. C., Guazzotti, S. A., Sodeman, D. A., Tang, Y., Carmichael, G. R., and Prather, K. A.: Mineral dust is a sink for chlorine in the marine boundary layer, Atmos. Environ. 41, 7166–7179, 2007.

Tegen, I. and Fung, I.: Modeling of mineral dust in the atmosphere: Sources, transport, and optical thickness, J. Geophys. Res.-Atmos., 99, 22897–22914, 1994.

Tegen, I., Harrison, S. P., Kohfeld, K., Prentice, I. C., Coe, M., and Heimann, M.: Impact of vegetation and preferential source areas on global dust aerosol: Results from a model study, J. Geophys. Res.-Atmos., 107, AAC 14-1–AAC 14-27, 2002.

Thorez, J.: Practical Identification of clay minerals, edited by: Lellote, G., Dison, Belgique, 90 pp., 1976.

Valentin, C. and Bresson, L. M.: Morphology, génesis and classification of Surface crusts in loamy and Sandy soils, Geoderma, 55, 225–245, 1992.

Van der Watt, H. V. H. and Valentin, C.: Soil crusting: the African view. Soil Crusting, Chemical and Physical Processes, Advances in Soil Science, Lewin Publ., Boca Raton, USA, 301–38, https://horizon.documentation.ird.fr/exl-doc/pleins_textes/pleins_textes_5/b_fdi_31-32/35528.pdf (last access: 17 November 2023), 1992.

Weaver, C. J., Ginoux, P., Hsu, N. C., Chou, M.-D., and Joiner, J.: Radiative forcing of Saharan dust: GOCART model simulations compared with ERBE data, J. Atmos. Sci., 59, 736–747, 2002.

Yus-Díez, J., Pandolfi, M., González-Flórez, C., Escribano, J., Gonzalez-Romero, A., Ivancic, M., Rigler, M., Klose, M., Kandler, K., Panta, A., Querol, X., Reche, C., Pérez García-Pando, C., and Alastuey, A.: Quantifying variations in multi-wavelength optical properties of freshly-emitted Saharan dust from the Lower Drâa Valley, Moroccan Sahara, in preparation, 2023.

Zender, C. S., Newman, D., and Torres, O.: Spatial heterogeneity in aeolian erodibility: Uniform, topographic, geomorphic, and hydrologic hypotheses. J. Geophys. Res.-Atmos., 108, 4543, https://doi.org/10.1029/2002JD003039, 2003.

Zender, C. S., Miller, R. L., and Tegen, I.: Quantifying mineral dust mass budgets:Terminology, constraints, and current estimates, Eos T. Am. Geophys. Un., 85, 509–512, https://doi.org/10.1029/2004EO480002, 2004.

Proof only